NASA-TP-2371 19850022829

Adaptive Identification and Control of Structural Dynamics Systems Using Recursive Lattice Filters

N. Sundararajan,
Raymond C. Montgomery,
and Jeffrey P. Williams
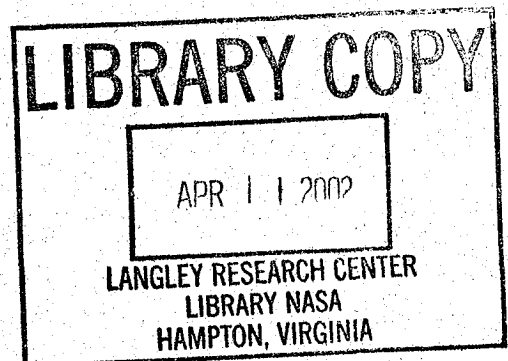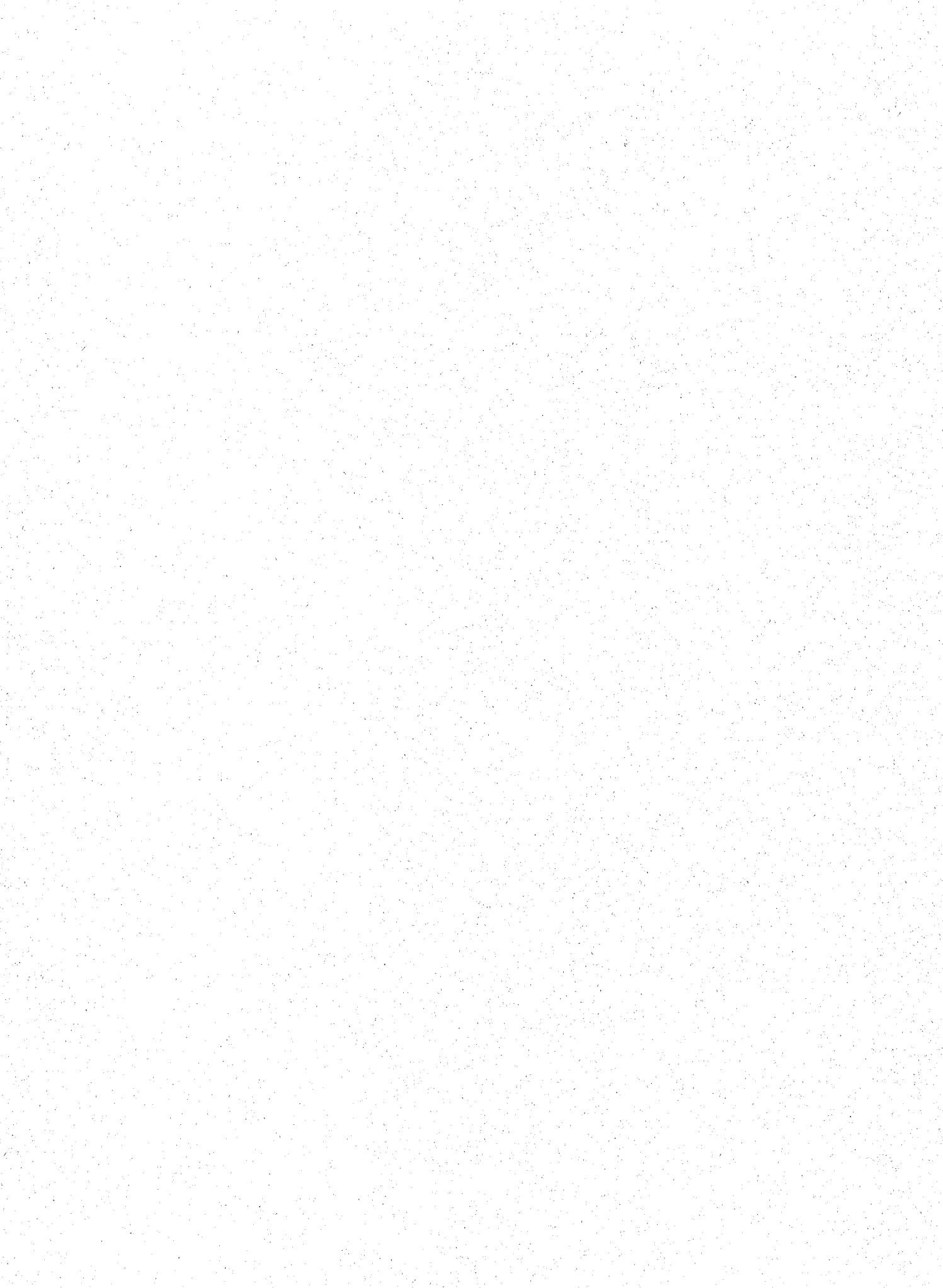
NASA

Adaptive Identification and Control of Structural Dynamics Systems Using Recursive Lattice Filters

N. Sundararajan,
Raymond C. Montgomery,
and Jeffrey P. Williams

Langley Research Center
Hampton, Virginia

Symbols

A_1, A_2, B_1, B_2	autoregressive moving average (ARMA) model parameters
$\mathcal{B}$	Bayes risk function (see eq. (9))
$\mathbf{C}$	weighting matrix
C_{ij}	cost of selecting hypothesis H_i when H_j is true
C_1, C_2, D_1, D_2	controller gains
E	expectation operator
$\mathcal{E}$	orthogonal projection operator
e	equation error
$\underline{e}$	normalized forward residual
$e_{i,n}$	forward residual (with i representing time and n representing order)
$\mathbf{f}$	actuator force vector, lb
H_i	hypothesis i
i, j, k, n	time instants
$k_{i,n+1}$	reflection coefficient
N	number
NM	number of modes
NS	number of sensors
NW	data-window size
$\mathbf{n}_k$	random noise vector, $NS \times 1$
p	probability
$\mathbf{q}$	modal amplitude vector, $NM \times 1$
$\mathbf{R}$	noise-covariance matrix
$r_{i,n}$	backward residual (with i representing time and n representing order)
$\underline{r}$	normalized backward residual
s	Laplace variable
$\mathbf{u}$	modal control force vector, lb
Y_i^n	subspace spanned by vectors $(y_i, y_{i-1}, \cdots, y_{i-n+1})$
$\mathbf{y}_k$	measurement vector, $NS \times 1$
$\hat{\mathbf{y}}_n$	linear least-squares estimate of $\mathbf{y_n}$
Z_i	decision region in observation space
z^{-1}	time-delay operator
α	random variable
ς	damping ratio
μ	scalar weighting factor in equation-error identification method
σ	standard deviation of measurement noise
σ_{conv}	parameter-convergence threshold
σ_{error}	fit-error threshold
σ_{inf}	information threshold
τ	sampling period, sec
τ_i	decision function
$\mathbf{\Phi}$	mode-shape matrix, $NS \times NM$
ω	natural frequency, rad/sec

Superscript:

T	transpose

Abbreviations:

ARMA	autoregressive moving average
A/D	analog/digital (see fig. 1)
D/A	digital/analog (see fig. 1)
DFT	discrete Fourier transform
LMS	least mean squares
LQG	linear quadratic Gaussian method
LSS	large space structures
VLSI	very large scale integration

Notation:

det	determinant
$\langle \cdot, \cdot \rangle$	inner product
$\| \ \|$	Euclidean norm
$\perp$	is orthogonal to
$\oplus$	direct sum
$\subset$	is contained in
$\hat{\ }$	estimate of

Summary

This report presents the application of recursive, least-squares lattice filters that are widely used in signal processing for adaptive identification and control of structural dynamics systems. The theory behind identification using lattice filters, the method for control by modal pole placement, and on-line validation procedures for properly integrating the identification and control are presented. The methods are illustrated by computer simulation for both a one-dimensional free-free beam and a two-dimensional flexible-grid structure. The results are then verified by using the experimental facility for both structures at the Langley Research Center.

Introduction

The dynamics and control of large space structures (LSS) is essentially a distributed parameter system problem. However, for a practical control-systems design, modal and finite-element analyses are used with the subsequent application of modern control-theory tools to a truncated, finite-order design model. Problems which arise in this process include the following:

(1) Design-model order: Since the original system has infinite dimensions, the number of modes to be selected in the design model for adequate control design is difficult to determine. If a high order is selected, computational and hence onboard implementation problems arise. Conversely, if a low order is selected, the resulting system may not satisfy performance requirements.

(2) Knowledge of model parameters: With detailed analysis and ground testing, the dynamic characteristics of a structure may be estimated; however, once it is in orbit, its characteristics may be quite different because of environment, construction anomalies, and other unforeseen factors. Different adaptive control methods have been proposed to overcome these problems (refs. 1 to 3).

(3) Number of required configurations: A large number of configurations may be required for LSS in orbit, and the design model required for each configuration may be different (ref. 4). Hence, the controller may be different both in order as well as gains. Since both order and gains may change, a gain scheduling method may not be suitable.

For these reasons, an adaptive control system for LSS is highly desirable. The system should be capable of on-line identification of the required design-model order, mode shapes, frequencies, and damping. Based on these identified parameters, the system should also be capable of on-line controller design and implementation that can guarantee stability and desired performance. In this report, an adaptive control system is proposed that

includes these capabilities. The system order, mode shapes, and modal amplitudes are estimated on line by using an identification method based on recursive, least-squares lattice filters (ref. 5). By using the identified model parameters, a modal control law based on a pole-placement method with the objective of vibration suppression (ref. 6) is employed.

The closed-loop distributed adaptive control studied in this report is shown in figure 1. The function corresponding to each block of figure 1 is described as follows: The lattice filter on the front end provides an on-line estimate of the system order, mode shapes, and modal amplitudes. This is carried out by using the modified Gram-Schmidt procedure involving both forward and backward residuals, in which the backward residuals form an orthonormal basis for the entire observation sequence. Also, the orthonormal basis functions generated by the lattice filter provide the mode-shape information. Although the basis functions from the lattice filter form an orthonormal set, they are not the natural modes but are linear combinations of them. Hence, the modal amplitudes constructed by using these basis functions will generally have spectral components of more than one natural mode. Since the ultimate objective is to provide a method of obtaining the natural mode-shape functions required for implementation of the modal control method of reference 6, a method of decoupling the modal amplitudes by transforming the basis functions obtained from the lattice filter has been developed (ref. 7). After obtaining the decoupled modes, the control-law design is carried out independently for each mode.

To accommodate digital implementation, an autoregressive moving average (ARMA) description of the modal dynamics is used. In order to calculate controller gains, the parameters of this model must be identified based on the time series of decoupled modal displacements generated by the lattice filter. This is accomplished through an equation-error identification method for determining the ARMA parameters (ref. 8). In order to make the closed-loop adaptive control stable and meet the performance requirements, a procedure for integrating the identification and control methods is developed. The identified parameters are processed through a series of test and validation procedures. The tests consist of checking for the fit error, convergence of parameters, and the amount of information in the measurement data. In figure 1, the block marked "Parameter identification and testing" represents these functions.

When the identified parameters pass all the tests, the controller gains are updated and the modal control forces are computed. For each mode, the control law used is based on a discrete-time pole-placement method that allows exact pole placement of system poles when

the modal parameters are known and the number of actuators is equal to the number of controlled modes (ref. 6). Even though pole-placement control law is used here, any other control method like the linear quadratic Gaussian (LQG) method can be used for design. By using the estimated mode shapes from the lattice filter, these modal control forces are converted to actuator forces and the entire adaptive control loop is closed.

The adaptive identification and control using the lattice filters proposed previously are illustrated first by simulations for a free-free beam and then for a more complex two-dimensional free-free grid structure. The identification results obtained for these two structures by simulations are then compared with those obtained from the experimental data for these structures at the Langley Research Center. The full closed-loop adaptive control method as shown in figure 1 is also studied by using simulations for both structures.

Elements of Lattice-Filter Theory

Lattice filters have found wide acceptance in the fields of adaptive signal and speech processing (ref. 9). Reference 10 is a comprehensive tutorial on the theory and applications of lattice filters. Lattice-filter theory simultaneously provides the tools required to select model order appropriately and determine the mode shapes. In all cases familiar to the authors, the order of the model is assumed a priori and the lattice filter is then used for the identification of the parameters of an autoregressive (AR) model. The novelty of the present report is that the model order is determined, on line, by using statistical multiple-decision theory (ref. 11). The main idea in this approach is that the system outputs contain all the information about its natural modes and that the complete system behavior can be characterized by a set of orthonormal functions derived from the outputs through a modified Gram-Schmidt procedure. The lattice filter provides an order as well as a time recursive algorithm for generating an orthonormal basis for the measurement data by using the most recent measurement samples. Herein, a method is presented to add an orthogonal function to the already existing basis functions if the measurement samples contain new significant information. The decisions to increase, maintain, or decrease the model order are based upon hypothesis-testing criteria. Such testing methods have been used for failure accommodation in the design of an aircraft digital flight control system (ref. 12). After the identification of the appropriate ARMA model is accomplished via recursive filters, the model is used for control purposes. The concept of orthogonal projections in a general real Hilbert space setting has been presented in reference 13. The procedure is a modified Gram-Schmidt procedure involving both forward and backward residuals, in which the backward residuals form an orthogonal

basis for the entire observation sequence. Hence, any least-squares estimate is the orthogonal projection onto this basis.

The immediate interest herein is to provide an efficient means for order and mode-shape determination for the adaptive control methods set forth in references 1, 3, and 14. For that purpose, assume that the ith measurement sample is of the form

$$y_i^T = [y^1(i), y^2(i), \ldots, y^{NS}(i)]$$

where the superscript NS represents the number of sensors. It is assumed that y is generated from a model wherein

$$\mathbf{y}_i = \Phi \mathbf{q}_i + \mathbf{n}_i \qquad (1)$$

Here, Φ is a $NS \times NM$ mode-shape matrix, $\mathbf{q}_i$ is the $NM \times 1$ modal-amplitude vector, and $\mathbf{n}_i$ is a $NS \times 1$ Gaussian random variable with zero mean and a covariance matrix $\mathbf{R}$. Typically, for structural dynamics applications, each component of $\mathbf{q}_i$ is the output of an uncoupled second-order process. The task here is to estimate the order and obtain the least-squares estimate of $\mathbf{q}_i$ and Φ from $N + 1$ measurement samples $\mathbf{y}_0$ through $\mathbf{y}_N$ depicted in figure 2. For the purpose of analysis, we will find it expedient to embed the problem in a set of problems of finding the estimate of $\mathbf{y}_i$ based on the measurements (that is, $\mathbf{y}_{i-n}, \ldots, \mathbf{y}_{i-1}$). Let Y_i^n be the space spanned by the n measurements up to and including $\mathbf{y}_i$. (See fig. 2.) The forward and backward residuals are the errors in estimating the measurements adjacent to the sample spaces defined in figure 2. For example, by referring to figure 1, the estimation of $\mathbf{y}_i$ based on the space Y_{i-1}^n is a forward estimation and produces an error

$$e_{i,n} = \mathbf{y}_i - \mathcal{E}(\mathbf{y}_i | Y_{i-1}^n) \qquad (2)$$

where $\mathcal{E}(\mathbf{y}_i | Y_{i-1}^n)$ is the orthogonal projection of $\mathbf{y}_i$ on the Y_{i-1}^n subspace. Correspondingly, the estimation of $\mathbf{y}_{i-n}$, based on the space Y_i^n, produces a backward estimate with an estimation error (residual)

$$r_{i,n} = \mathbf{y}_{i-n} - \mathcal{E}(\mathbf{y}_i | Y_{i-1}^n) \qquad (3)$$

Clearly, the backward residuals $r_{i,n}$ for $n = 0, 1, \ldots, i$ are orthogonal and form a basis for the space Y_i^n. Note however that this is not true for the forward errors $e_{i,n}$.

We will now seek formulas that relate order n and time i recursions for the forward and backward residuals. Rewriting equation (2) for the case where n is replaced by $n + 1$ results in

$$e_{i,n+1} = \mathbf{y}_i - \mathcal{E}(\mathbf{y}_i | Y_{i-1}^{n+1})$$

Solving for $\mathbf{y}_i$ in equation (2) and substituting in the last equation results in

$$e_{i,n+1} = e_{i,n} + \mathcal{E}(\mathbf{y}_i | Y_{i-1}^n) - \mathcal{E}(\mathbf{y}_i | Y_{i-1}^{n+1})$$

Now, the space Y_{i-1}^{n+1} can be written as

$$Y_{i-1}^{n+1} = Y_{i-1}^n \oplus \mathbf{y}_{i-n-1} = Y_{i-1}^n \oplus r_{i-1,n}$$

where $\oplus$ represents the direct sum of two spaces. This follows since $r_{i-1,n}$ is the component of $\mathbf{y}_{i-n-1}$ that is not in the space Y_{i-1}^n. Hence,

$$\mathcal{E}(\mathbf{y}_i | Y_{i-1}^{n+1}) = \mathcal{E}(\mathbf{y}_i | Y_{i-1}^n) + \mathcal{E}(\mathbf{y}_i | r_{i-1,n})$$

so that

$$e_{i,n+1} = e_{i,n} - \mathcal{E}(\mathbf{y}_i | r_{i-1,n}) \qquad (4)$$

We may substitute for $\mathbf{y}_i$ from equation (2) to simplify the last term and obtain

$$\mathcal{E}(\mathbf{y}_i | r_{i-1,n}) = \mathcal{E}\left\{ \left[e_{i,n} + \mathcal{E}(\mathbf{y}_i | Y_{i-1}^n) \right] | r_{i-1,n} \right\}$$

and since $\mathcal{E}(\mathbf{y}_i | Y_{i-1}^n) \subset Y_{i-1}^n$ and $r_{i-1,n} \perp Y_{i-1}^n$, the last term on the right-hand side vanishes and

$$\mathcal{E}(\mathbf{y}_i | r_{i-1,n}) = \mathcal{E}(e_{i,n} | r_{i-1,n})$$

Hence, equation (4) becomes

$$e_{i,n+1} = e_{i,n} - \mathcal{E}(e_{i,n} | r_{i-1,n}) \qquad (5)$$

A similar argument may be used to derive a recursion formula for r yielding

$$r_{i,n+1} = r_{i-1,n} - \mathcal{E}(r_{i-1,n} | e_{i,n}) \qquad (6)$$

Note the similarities in the last two equations and the time shift in the latter.

Equations (5) and (6) are the basic recursion formulas needed for constructing a lattice-filter algorithm. By referring to figure 3 we may, in fact, write the least-squares estimate of $\mathbf{y}_N$ based on the space Y_{N-1}^n by noting that $r_{N-1,j}$ for $j = 0, 1, \ldots, n-1$ is a basis for Y_{N-1}^n so that

$$\hat{\mathbf{y}}_N = \hat{\mathbf{y}}_N(Y_{N-1}^n) = \mathcal{E}(\mathbf{y}_N | Y_{N-1}^n)$$
$$= \sum_{j=0}^{n-1} \mathcal{E}(\mathbf{y}_N | r_{N-1,j})$$

Substitution for $\mathbf{y}_N$ from equation (2) with n replaced by N yields

$$\hat{\mathbf{y}}_N = \sum_{n=0}^{N-1} \mathcal{E}\left\{ \left[e_{N,n} + \mathcal{E}(\mathbf{y}_N | Y_{N-1}^n) \right] | r_{N-1,n} \right\}$$

Again, since $\mathcal{E}(\mathbf{y}_N | Y_{N-1}^n) \subset Y_{N-1}^n$ and $r_{N-1,n} \perp Y_{N-1}^n$, the last term on the right-hand side vanishes and we have

$$\hat{\mathbf{y}}_N = \sum_{n=0}^{N-1} \mathcal{E}(e_{N,n} | r_{N-1,n}) \qquad (7)$$

Equations (5), (6), and (7) represent the lattice-filter algorithm in a general real Hilbert space setting. A normalized form of these equations may be derived by using the inner-product form of the projection operator

$$\mathcal{E}(a|b) = \frac{\langle a, b \rangle}{\langle b, b \rangle} b$$

where a and b are nontrivial elements of the Hilbert space and where $\langle a, b \rangle$ is their inner product. Normalizing the e and r residuals results in unit vectors $\underline{e}$ and $\underline{r}$, respectively, satisfying

$$\underline{e}_{i,n} = \frac{e_{i,n}}{\langle e_{i,n}, e_{i,n} \rangle}$$

$$\underline{r}_{i,n} = \frac{r_{i,n}}{\langle r_{i,n}, r_{i,n} \rangle}$$

Equations (5) and (6) can be written in terms of $\underline{e}$ and $\underline{r}$ resulting in

$$\underline{e}_{i,n+1} = (1 - k_{i,n+1}^2)^{-1/2}(\underline{e}_{i,n} - k_{i,n+1} \underline{r}_{i-1,n})$$

$$\underline{r}_{i,n+1} = (1 - k_{i,n+1}^2)^{-1/2}(\underline{r}_{i-1,n} - k_{i,n+1} \underline{e}_{i,n}) \qquad (8)$$

wherein

$$k_{i,n+1} = \langle \underline{e}_{i,n}, \underline{r}_{i-1,n} \rangle$$

The symmetry of the recursion formulas is now apparent. The equations are coupled by the term $k_{i,n+1}$, which is customarily called the reflection coefficient. The structure of this equation is depicted in figure (4) in which we have used the symbol z^{-1} to represent the time-shift operator. That is,

$$z^{-1} r_{i,n} = r_{i-1,n}$$

The lattice filter derives its name from this structure. The lattice-filter form has the following advantages:

1. Given a basis for order N, a basis for order $N + 1$ can be obtained by using the recursive formulas given previously in equation (8).

2. Because of the modified Gram-Schmidt procedure, the basis for all orders n between 0 and N are the first n elements of the basis of order N.

3. The estimate assuming any order n between 0 and $N + 1$ can be computed by using equation (7).

Thus, the lattice filter provides the information needed to determine the residual sequence for any model order between 0 and $N + 1$ inclusive. This information provides the basis for the model-order determination presented in the next section.

Model-Order Determination

In this section we develop a method for selecting the model order (between 0 and $N + 1$) that is optimal

with respect to a Bayes risk function. When a new measurement is processed, the order of the system can be increased, decreased, or maintained as before. The reduction in order can be of any size, whereas the increase in order is by 1.

The method is based on multiple hypothesis testing of $N + 2$ hypotheses where hypothesis H_i corresponds to a system of order i for i values between 0 and $N + 1$. Thus, the hypothesis H_i corresponds to

$$\mathbf{y}_i = \boldsymbol{\Phi}\mathbf{q}_i + \mathbf{n}_i$$

where $\boldsymbol{\Phi}$ is of rank i. Based on a set of measurements, $Y(NW) = [y(1), y(2), \ldots, y(NW)]$ where NW represents the data-window size. The most probable hypothesis for the system is selected by minimizing the Bayes risk function defined by

$$\mathcal{B} = \sum_{i=0}^{N+1} \sum_{j=0}^{N+1} C_{ij} P_{H_j} \int_{Z_i} P_{y|H}(\alpha|H_j)\, d\alpha \qquad (9)$$

where P_{H_j} represents the a priori probability of hypothesis H_j being true, C_{ij} is the cost of selecting H_i when H_j is true, and $P_{y|H}(\alpha|H_j)$ is the conditional probability density of measurement y when H_j is true. The symbol $\int_{Z_i}$ implies that the integral is carried out over the decision region Z_i in the observation space. Decision regions Z_i are subsets of observation space such that if y is in Z_i, then the hypothesis H_i is to be selected. Note that the integral in equation (9) represents the probability of making the incorrect decision of selecting hypothesis H_i when H_j is true for $i \neq j$. So, the Bayes risk function $\mathcal{B}$ represents the sum of probabilities corresponding to different decisions weighted by the a priori probabilities P_{H_j} and the design weights C_{ij}. The problem then is to choose the boundary of decision regions Z_i that will result in the minimum Bayes risk function. This minimization can be accomplished by selecting the hypothesis that produces the minimum:

$$\mathcal{B} = \sum_{i=0}^{N+1} \int_{Z_i} \tau_i(\alpha)\, d\alpha$$

where

$$\tau_i(\alpha) = \sum_{j=0}^{N+1} C_{ij} P_{H_j} P_{y|H}(\alpha|H_j) \qquad (10)$$

The Bayes risk function is minimized by selecting H_i at each point α in the observation space so that $\tau_i(\alpha)$ is the smallest of its $N + 1$ possible values. Hence, the optimal decision regions are, for all j,

$$Z_i = [\alpha | \tau_i(\alpha) < \tau_j(\alpha)]$$

The computation of $p(\alpha|H_j)$ is based on the assumption of a Gaussian noise process so that

$$p(\alpha|H_j) = \frac{1}{(\det \mathbf{R})^{1/2}} \exp\left(-\frac{1}{2} r^T \mathbf{R}^{-1} r\right)$$

where $r = \alpha - \bar{\alpha}$ for each measurement sample. Further, since the noise process is assumed to be white, the chain rule of probabilities reduces to

$$p(\alpha|\mathrm{H_j}) = \frac{1}{\left(\det \prod_{k=1}^{NW} \mathbf{R}\right)^{1/2}} \exp\left(-\frac{1}{2} \sum_{k=1}^{NW} e_{k,j}^T \mathbf{R}^{-1} e_{k,j}\right)$$

in which a data window of NW samples is used in the decision process. In the last equation we have used the forward residual e taken from equation (2) where (i, n) is replaced by (k, j). Note that the minimization of τ and, hence, the optimal decision for the system order depends on the choice of weighting matrix $\mathbf{C}$ and on the a priori probabilities. These parameters can be selected depending on one's objectives. If one has a priori knowledge about the system (say, its order), then $\mathbf{C}$ and P_H can be selected to reflect this. Also, if one wants the selected model order to be greater than or equal to the true model order, the $\mathbf{C}$ matrix can be selected with the upper diagonal elements being greater than the respective lower ones. These options are illustrated in simulation examples to follow.

Clearly, in this approach one may "fit the noise" by continually increasing the order of the system; however, once the order of the estimator has increased beyond the correct order, then the residual errors should lie within a noise band which can be predicted based on assumed noise characteristics. A threshold can be selected based on this predicted noise band, and the order can be determined by a test of whether the residuals have been reduced to lie within the noise band. The residuals will generally consist of signal and noise parts, with the signal part being reduced as the correct order is reached until the residuals essentially consist only of noise. Thus, for sufficiently large $\mathbf{n}$,

$$E \sum_{i=1}^{NW} e_{i,n}^T e_{i,n} = NW \, E(\mathbf{n}_i^T \mathbf{n}_i)$$

$$= NW \, tr \, E(\mathbf{n}_i \mathbf{n}_i^T) = NW \sum_{j=1}^{NS} \sigma_j^2$$

where E is the expectation operator and tr represents the trace. This can be used as the 1σ threshold for the order-determination test. In the last equation, σ_j is the standard deviation of the noise process for the jth sensor.

Computational Requirements

In order to give an insight into the computational complexities involved in using the lattice-filter algorithms, a comparison with other least-squares methods is given in the following table (ref. 10). A rough comparison of the different algorithms can be achieved by counting the number of arithmetic operations (including multiplication, division, and addition) needed to carry out the operations. The count is made for an Nth-order predictor.

Method	Number of operations
Block processing; prediction error method	$5N$
Fast Kalman; recursive least squares	$8N$
Gradient least mean squares (LMS)	$2N$
Gradient lattice (two coefficients)	$10N$
Unnormalized least-squares lattice	$10N$ ($3N$ division)
Normalized least-squares lattice	$12N$ ($3N$ square roots; $4N$ division)

Compared with other methods, the lattice method generates estimates for all orders up to and including N at the same time. If there is a need for an on-line order determination, the lattice filter offers an ideal choice. For example, in comparison with the fast Kalman method, if the order N is greater than 2 and one needs estimates for all orders up to N at the same time, then the lattice-filter method offers a smaller number of computations.

The comparison based on number of operations should be considered with some caution since there are other issues involved. For example, the normalized lattice filter has the potential of fixed-point implementation because of the fact that all internal variables are less than 1 in magnitude. Also, the normalized lattice recursions can actually be expressed as a sequence of circular and hyperbolic rotations. Efficient computation of these rotations can be achieved by the use of the Coordinate Rotation Digital Computer (CORDIC). The possibility of performing the basic lattice recursions by using special-purpose hardware (e.g., a very large scale integration (VLSI) chip) makes the number of operations less important than, say, the architecture of the computations. (See ref. 10.)

Spectral Decoupling of Lattice-Filter Basis Functions

The adaptive control method proposed in this study (see fig. 1) is based on modal decomposition and requires a set of uncoupled modes for implementation. Lattice filters form an orthonormal basis from the measurement samples by using a modified Gram-Schmidt procedure. Since the basis functions are orthonormal, they may be easily added or deleted, and hence, the model order can be easily increased or decreased. Although the basis functions form an orthonormal set, they are not the natural modes but are linear combinations of them. Hence, the modal amplitudes constructed by using these basis functions will generally have spectral components of more than one natural mode. Thus, the modal amplitudes obtained through a direct application of lattice filters are coupled.

In this section a method is presented for decoupling the modal amplitudes by transforming the basis functions obtained from the lattice filter (ref. 7). The ultimate objective is to provide a method of obtaining the mode-shape functions required for implementation of the adaptive control method of figure 1. The previous section presented a method for estimating the number of independent modes present in the output measurements. Lattice filters were used to obtain the least-squares estimate of the measurements based on the last n time samples, with n being the order estimate. The criterion used for the order estimate was that the estimation residuals lie within a band determined from assumed sensor noise characteristics. The lattice filter was operated at a fixed order but continued updating the orthonormal basis at each time sample so that the current basis corresponds to that required for the last n time samples. Note that this approach produces a different set of basis functions (or modes) at each time sample.

In the present work, when the order estimate is constant, a fixed set of basis functions that are spectrally decoupled is required to carry out identification and control. Because of this requirement, a fixed orthonormal basis is used during intervals when the order estimate is constant. (However, the order estimate is checked at each measurement sample based on the threshold test.) The method is a frequency domain approach that utilizes the discrete Fourier transform (DFT). The lattice filter uses the current measurement as the first mode shape and, by using a modified Gram-Schmidt orthonormalization procedure, generates additional basis functions from estimation residuals. Consequently, the output of the lattice filter produces coupled mode shapes and corresponding modal amplitudes in which the first coupled modal amplitude will contain all significant natural modes.

The theory of reference 5 is used to provide an estimate of the order of the process n. Thus, the first coupled mode DFT amplitude spectrum is searched for the n most significant peaks and corresponding frequencies. Because the spectrum contains n peaks for the n frequencies, a transformation matrix can be obtained that decouples the spectrum. This transformation matrix is the inverse of the matrix whose elements are the real parts of the transforms of the n coupled modal amplitude channels (rows) evaluated at the n peak frequencies (columns). After the transformation matrix is determined, the coupled mode shapes are decoupled by using the same transformation matrix. Some of the limitations associated with obtaining the natural modes by decoupling from lattice basis functions are presented in the following discussion.

To provide a fine frequency resolution, the number of points in the DFT data base have to be increased or the sampling rate has to be increased. If the modes are closely spaced, this may pose a problem.

Since the decoupling is based on the real part of the Fourier transform, the phase information between the different lattice modes is not considered in the transformation. Incorporation of this phase information, although straightforward, will result in a complex transformation. This involves scaling and time shifting of the different lattice modes in time domain to obtain decoupling. Neglecting the phase information for structures with near-zero damping is reasonable. An alternate method of avoiding this transformation is to carry out an eigenanalysis of the ARMA model obtained from the lattice filter to obtain the natural modes. A better solution is to use the ARMA model estimated from the lattice filter directly into the controller design. These aspects are not considered in this report. In this study, the adaptive control method is tested by using the mode shapes obtained previously from the lattice filter and also from the analytic prediction of the natural modes of the structural dynamics system. Based on the decoupling transformation, the decoupled modal amplitude time series is then analyzed for each mode to identify the parameters of its ARMA model.

ARMA Parameter Identification

The objective of the identifier is to determine the coefficients in the second-order ARMA model of the lattice-filter decoupled modal-amplitude time series $q(k)$. The method is based on an equation-error method described in references 1 and 8. For each mode in figure 1, the model is described by the equation

$$q(k-1) = A_1 q(k-2) + A_2 q(k-3) + B_1 u(k-2)$$
$$+ B_2 u(k-3) \qquad (11)$$

where u represents the modal control force. The equation error is given by

$$e(k-1) = q(k-1) - \hat{q}(k-1)$$

$$\hat{q}(k-1) = \hat{A}_1 q(k-2) + \hat{A}_2 q(k-3)$$
$$+ \hat{B}_1 u(k-2) + \hat{B}_2 u(k-3)$$

where $\hat{q}$ is the modal amplitude estimated by the lattice filter, k is the sample number, and $\hat{A}_1$, $\hat{A}_2$, $\hat{B}_1$, and $\hat{B}_2$ are the ARMA coefficients. The ARMA coefficients are then updated by

$$
\begin{bmatrix} \hat{A}_1(k) \\ \hat{A}_2(k) \\ \hat{B}_1(k) \\ \hat{B}_2(k) \end{bmatrix}
= \begin{bmatrix} \hat{A}_1(k-1) \\ \hat{A}_2(k-1) \\ \hat{B}_1(k-1) \\ \hat{B}_2(k-1) \end{bmatrix}
+ e(k-1)\mu \begin{bmatrix} q(k-2) \\ q(k-3) \\ q(k-1) \\ u(k-2) \end{bmatrix}
$$

The weight μ assures stability if (ref. 8)

$$0 < \mu < 2| \left[q^2(k-2) + q^2(k-3) + u^2(k-2) \right.$$
$$\left. + u^2(k-3) \right]$$

This identifier performs well in a low-noise environment; but when the information content of the signal is small, it attempts to fit the noise (ref. 14). Also, the ideal ARMA model for the beam has input parameters (B) which are three orders of magnitude smaller than the model parameters (A). This causes a very high sensitivity to noise in the identification of B; and when the input force is applied, it tends to cause the identifier gain on A to decrease significantly. Although these effects are evident in the results presented here, they did not prevent successful identification.

If one is interested in determining the damping ratios and natural frequencies of the modes, they can be obtained in a straightforward manner from equation (11). However, it should be noted that this is not unique because of the foldover phenomenon due to sampling. By finding the roots of equation (11) and using the relation $z = e^{s\tau}$ in the primary strip, where τ is the sampling period, the following equations for natural frequency and damping ratio are obtained, respectively:

$$\omega = \theta/2\pi\tau$$

$$\varsigma = C(C^2 + \theta^2)^{1/2}$$

where

$$\theta = \tan^{-1} b/a$$

$$C = -\frac{1}{2}\ln(a^2 + b^2)$$

and

$$a = \text{Real}(z_r)$$

$$b = \text{Imaginary}(z_r)$$

where z_r pertains to the roots of equation (11) in the z-domain. The behavior of this overall system-identification methodology with experimental data is discussed in the subsequent sections.

Modal Control Law

The control method used here is based on a modal decomposition of the sensor outputs. The closed-loop design objective is to suppress the vibrations of each controlled mode. To achieve this, the modal control method described in references 1 and 6 is used to calculate control gains that will place the roots of the open-loop undamped system onto a constant damping line. This pole-placement objective is specified in the frequency domain and then converted to the discrete z domain by the transformation $z = e^{s\tau}$, where τ is the sampling period. The control law that will place the poles at the desired locations is calculated by assuming a control law that takes the same form as the equations of motion:

$$\mathbf{u}(k) = C_1\mathbf{q}(k-1) + C_2\mathbf{q}(k-2) + D_1\mathbf{u}(k-1) + D_2\mathbf{u}(k-2)$$

The control gains C_1, C_2, D_1, and D_2 are calculated on line. Note that this law requires only the feedback of modal amplitudes. The velocity feedback needed to provide proportional viscous-type damping is embedded in the difference of successive displacements. By transforming the equations of motion and control to the z-domain, the closed-loop characteristic equation can be written as

$$z^4 + (-A_1 - D_1)z^3 + (D_1A_1 - A_2 - D_2 - B_1C_1)z^2$$
$$+ (D_1A_2 + D_2A_1 - B_1C_2 - B_2C_1)z$$
$$+ (D_2A_2 - B_2C_2) = 0$$

which we note is a fourth-order algebraic equation. Two of its roots are specified by the closed-loop design requirements, whereas the remaining two roots are discretionary. These discretionary roots may be selected by the designer to improve the closed-loop characteristics relative to noise suppression or robustness to parameter uncertainty. In this study, these two discretionary roots had the same frequency as the design roots but additional damping was introduced to avoid repeated roots. Given the four characteristic roots, one may construct a desired characteristic equation and, by equating its coefficients with those of the last equation, obtain four equations in the four unknown control gains C_1, C_2, D_1, and D_2.

Having calculated the modal control forces according to the aforementioned control law, the actuator forces are determined by solving

$$\Phi^T\mathbf{f} = \mathbf{u} \qquad (12)$$

where Φ is the mode-shape matrix determined by the transformation algorithm and $\mathbf{f}$ and $\mathbf{u}$ are the vectors of actuator and generalized modal forces, respectively. Note that if the number of modes controlled is more than the number of actuators, a least-squares fit must

be used and the exact closed-loop poles will not be realized. Since the control gains are dependent on the identified parameters, improper identification will prevent the design goals from being met. Sensitivity of closed-loop stability to parameter error was studied in reference 6 to determine parameter-accuracy requirements for the identifier. The study of reference 6 showed that when the solution of equation (12) is exact, stability will be maintained for parameter errors of ±12 percent in mode 3 and up to ±30 percent in mode 4. These studies were made for an ideal case with no noise and no mode-shape errors; thus, these limits should be considered absolute maximums.

Parameter Testing

In the earlier sections, a method for identifying the ARMA model parameters from modal amplitude time series and a method for modal control using these parameters were described. Serious problems may arise if one directly integrates the identification and control methods if the identification method produces erroneous parameter values. Hence, before attempting control, one should check the validity and accuracy of the identified parameters. Also, if the signal from which identification is carried out does not contain enough information, it is unreasonable to expect the identified parameters to be accurate. One method for testing parameters would be simply to turn on the controller and observe the result. This is not a desirable approach in an on-line adaptive system. To overcome these problems, a series of test procedures which ensure the adequacy of identification before control is attempted are described subsequently. The technique used here is to test the parameter-identifier input signal and the identified parameters against some a priori criteria. The three tests used in this procedure pertain to the following:

(1) Model fit error
(2) Parameter convergence
(3) Signal information

Although we do not propose that this set is sufficient to guarantee proper identification, it does serve to illustrate the basic concepts of parameter testing and has been used successfully in experimental work.

The fit-error test uses a fixed parameter set to calculate an estimated modal amplitude for the past NW sample. These tests were run with NW arbitrarily set to 10. The equation for this test is

$$\sigma_{\text{error}} > \sum_{n=0}^{NW} \left| \mathbf{q}(k-n) - \left[\hat{A}_1\mathbf{q}(k-n-1) \right. \right.$$
$$+ \hat{A}_2\mathbf{q}(k-n-2) + \hat{B}_1\mathbf{u}(k-n-1)$$
$$\left. \left. + \hat{B}_2\mathbf{u}(k-n-2) \right] \right| \qquad (k > NW) \quad (13)$$

If the absolute sum of the error between the modeled amplitude and the displacement calculated by the ARMA model exceeds a given threshold, the fixed parameter set is updated with the present identified parameter set. This process is repeated until the parameter set fits the data. The convergence test runs concurrently with the fit test, and it simply checks the magnitude of the changes in successive estimated parameters. For $h = \hat{A}_1$, $\hat{A}_2$, $\hat{B}_1$, and $\hat{B}_2$, the equation is

$$\sigma_{\text{conv}} > \sum_{n=0}^{NW} |h_n - h_{n-1}| \qquad (14)$$

If the absolute sum of 10 successive changes in parameter estimates is above a specified level of σ_{conv}, the test indicates a failure and a logical switch is set to false.

The final test is on information content of the estimated modal amplitude signals from the lattice filters. The purpose of this test is to check whether enough information is present in the signal for proper identification of the parameters. If this test fails, the controller gains are not updated based on the identified parameters but are frozen at the last values before the test failed. Here, the estimated modal amplitudes and velocities from the lattice filter are checked for sufficient excitation by summing over 10 samples. Thus, the equation is

$$\sigma_{\text{inf}} < \sum_{n=0}^{NW} (|\hat{q}_n| + |\hat{q}_{n+1} - \hat{q}_n|) \qquad (15)$$

If the sum is below a threshold of σ_{inf}, the updating of the control gains based on the identified parameters is stopped. The control gains are kept frozen at the values obtained just before the tests failed.

When all tests for parameters of a given mode have passed, control gains are calculated according to the previously described pole-placement method. The information and fit-error tests (eqs. (13) and (15)) constitute one test for each mode, and the convergence tests (eq. (14)) constitute four tests for each mode. Thus, six tests must be passed before control is applied to a given mode. Note that if any one of the tests fail, the control-law design parameters are not changed. Hence, the control gains are kept frozen at the values obtained just before the tests failed. The actual stability and performance of the controller is directly affected by the criterion chosen for passing a test. If the test criterion is too stringent, system noise and nonlinearities may preclude initiation of control. However, if the tests are not adequate, it is possible that an error in the estimated parameters could result in gain calculations that produce an unstable system.

This theory developed for identification and adaptive control by using lattice filters is tested by using both simulation and experimental hardware, first for a free-free beam and then for a free-free grid structure. Results of these studies are presented in the following sections.

Identification and Adaptive-Control Studies for a Free-Free Beam

In this section, the lattice-filter theory developed earlier is illustrated for the identification and adaptive control of a free-free beam. The identification method yields the structural dynamic characteristics of the beam, and the objective of control is vibration suppression. For the identification, results are presented by using both digital simulation and the experimental hardware for the beam available at the Langley Research Center. The adaptive control results are presented by using simulations.

The experimental apparatus for the free-free beam, which is shown in figure 5, consists of a 12-ft beam of rectangular cross section that is suspended from the ceiling by two cables and is attached to four electromagnetic force actuators. There are nine noncontacting deflection sensors that measure the translational deflection of the beam. The arrangement of the equipment is schematically indicated in figure 6, which also shows the first three flexible modes and frequencies of the beam. The sensors are numbered 1 to 9 from left to right in figure 6. The actuators are compensated to eliminate the effects of friction as much as possible. This compensation is nonlinear and produces a force in the direction of the beam motion at the actuator attachment points that is designed to equalize the effect of friction. Further details of the experimental apparatus can be found in reference 15.

Simulation Results

The digital simulaton used herein is based on a finite-element analysis of the beam. The finite-element analysis was made with 25 equally spaced joints with 1 at each end of the beam. The analysis was made by constraining the motions to translation and rotation along an axis perpendicular to the axis of suspension. Figure 6 presents the modal frequencies obtained and the mode shapes for the vibration modes of interest as determined by the digital sample rates (32 Hz) that are available in the experimental apparatus. The hypothesis testing and threshold approaches presented in this paper were tested in the digital beam simulation for identifying the system order along with its parameters (mode shapes).

Hypothesis-Testing Simulations

In these studies of hypothesis-testing simulations, the effects of two different choices for the cost matrix **C**

on order estimation are illustrated. The a priori probabilities were assumed equal and the diagonal elements of the C matrix were assumed to be zero in these studies. In the first case, **C** was selected as

$$\mathbf{C} = \begin{bmatrix} 0 & 1 & 2 & 3 & \cdots \\ 0.5 & 0 & 1 & 2 & \cdots \\ 1 & 0.5 & 0 & 1 & \cdots \\ 1.5 & 1.0 & 0.5 & 0 & \cdots \\ \vdots & \vdots & \vdots & \vdots & \end{bmatrix}$$

This choice of **C** gives preference to having a model-order estimate greater than that of the true system rather than risking a lower one. Based on the theory developed in the section entitled "Model-Order Determination," the τ_L matrix (consisting of likelihood functions τ_i in eq. (10)) at measurement samples 2, 3, 4, and 5 is, respectively,

$$\tau_L^T = [1.43, \ 0.69, \ 0.62]$$

$$\tau_L^T = [2.73, \ 1.61, \ 0.85, \ 0.84]$$

$$\tau_L^T = [4.92, \ 3.19, \ 2.17, \ 1.81, \ 2.32]$$

$$\tau_L^T = [4.92, \ 3.12, \ 2.03, \ 1.65, \ 2.03]$$

Based on the minimization of τ_i, it is clear that the correct order is indicated as 4 after the fourth sample.

For the second case, the weightings of C_{ij} were reversed. It was assumed that it is better to have a lower model-order estimate than the true system order. This philosophy might be evoked if the order estimate approaches saturation of the computational system. The **C** matrix for this case is

$$C_{ij} = 0.5(j - i) \qquad (i < j)$$
$$C_{ij} = 0 \qquad (i = j)$$
$$C_{ij} = (i - j) \qquad (i > j)$$

The corresponding τ_L matrix at the same sample instants as those given earlier are

$$\tau_L^T = [0.25, \ 0.39]$$

$$\tau_L^T = [0.25, \ 0.23]$$

$$\tau_L^T = [0.74, \ 0.69, \ 1.35]$$

$$\tau_L^T = [0.73, \ 0.54, \ 1.05]$$

It is seen from these data that the model order is indicated as 2 even though the true system order was 4.

Thus, the choice of cost matrix **C** reflects the weights one wants to put on the hypothesis testing. If one has a priori knowledge, the C_{ij} and P_{H_j} elements can be selected to reflect this. In applying this algorithm a complication exists when there is a large amount of measurement noise. It is well-known that Gaussian white noise may be modeled as an infinite dimensional process. Hence, when a large amount of noise is present, the hypothesis-testing method will tend to increase the system order continually and "fit the noise." This tendency can be avoided if one implements the threshold test previously presented. Results of simulations undertaken by using this test are the subject of the next section.

Threshold-Test Simulations

Nominal case. For the nominal case two rigid-body and three flexible modes were used. The measurements were sampled at 32 Hz and were corrupted with Gaussian white noise that had a standard deviation of 0.005 in. In all studies, the initial conditions for all modal amplitudes were 0.05 and the modal velocities were 0. The data-window size was taken to be 4, and threshold tests were not started until enough measurement samples were taken to fill the window. This results in a continual increase in order estimate for the first NW samples. Figure 7 shows simulation results for the nominal case. Note that the order estimate increases for the first four samples and then oscillates between 4 and 5. Even though the system has five modes, with the initial conditions selected, the two rigid-body modes appear as a single zero-frequency mode and, hence, the correct order estimate should be 4. The second graph in figure 7 is the norm of all nine measurement residuals and indicates the fit of the model. The next curve is the residual of measurement 4. This is followed by the output of sensor 4. Sensor 4 data were selected for illustration and are typical of the remaining eight sensors shown in figure 6. In data processing, all nine sensors were used to determine the model order and the least-squares estimates on which the residual computations are based. From detailed simulation, it was found that the order oscillation seen in the figures occurs because of the inadequacy of sampling frequency compared with that of the highest mode natural frequency. For example, figure 8 shows the order variation for the cases with three and four modes in the simulation. From these simulations, it seems that at least one order of magnitude separation should exist between sampling frequency and the highest mode natural frequency.

With nominal results available, the effect of threshold selection on the order determination was studied. Instead of assuming a 3σ threshold as in the nominal case, the threshold was relaxed to 2σ and to 1σ levels. The results are summarized in figure 9. As anticipated, the 3σ threshold is most conservative, whereas for 2σ and 1σ the order shifts toward 5 and 6, respectively. A value of 3σ was selected for the nominal threshold. For all further studies, the nominal parameters are used except for the particular parameter being studied.

9

Effects of data-window size. In order to avoid the problem of sudden variations in order estimate, the test for order is carried out after accumulating the residuals for a data-window size of NW. Figure 10 presents the order time histories for the two cases in which the data-window size was 1 and 8. As anticipated, the order time history for $NW = 8$ is smoother that that for 1. The choice of window size for a particular problem is closely related to the measurement noise level and also to the sampling rate.

Effects of noise level. In the noise-free case, the method should lead to exact-order determination as indicated in figure 11. The figure also shows the case in which the noise standard deviation σ is 0.01 in., which is twice that of the nominal case. This increase in noise predictably affects the model-order estimate as shown. This effect can be reduced by increasing the data-window size, which essentially acts as an averaging process.

Effects of modal damping. The effects of including modal damping are that higher modes are caused to decay faster and hence reduce the order as time evolves. Figure 12 shows the effect of including damping for all five modes. The damping ratio for all modes was taken as 0.005. The resulting modal amplitude history is also shown. It is seen from the figure that the order estimate has a tendency to decrease.

Model-order tracking. In order to study the effectiveness of the proposed method, the system order was increased by 1 at time increments of 2 sec, starting from 1 sec. (The initial order was 2.) The system order was then checked as to whether the method correctly tracks it. Results of increasing the model order in this manner are shown in figure 13. It is seen that the method tracked the simulated system behavior. For the decreasing order study, the initial order was set at 5; and at every time increment of 2 sec, starting from 1 sec, the order was reduced by 1. From figure 13, it is seen that the method tracks the order reduction as well as the order increase.

Decoupling Application to Free-Free Beam

The decoupling technique presented has been tested by using a simulation of a free-free beam described previously. One rigid body and three flexible modes were used in the simulation studies. Figure 14 shows time histories of the first two coupled modal amplitudes obtained from the lattice filters. Figure 15 shows the corresponding spectrum for all modes simulated with peaks at frequencies corresponding to the rigid (zero) and first three elastic modes. The decoupling transformations were obtained by using a DFT data base of 256 time samples at 32 Hz. The resulting decoupled modal amplitudes and the corresponding spectrum are also shown in figures 14 and 15, respectively. It is seen

from these figures that the technique works well for this case.

Experimental Results For Free-Free Beam

In this section, the experimental results for the identification for the dynamics free-free beam are presented (ref. 15). Testing was done by manually exciting the beam approximately in its first flexible mode and sampling the 9 sensors at 64 samples per second. A total of 5 sec of data were stored on a tape which was post processed with the algorithm.

Figure 16 shows a time history of some of the measurement data processed by the algorithm. The sensors are numbered sequentially from the left, as shown in figure 6. The innovations (INOV) sequence for sensor 4 is shown just below its time history. Also shown is the estimation norm (ENORM) of the forward residual, which includes all components of the measurement vector. Below the norm is the estimate of model order. This was obtained by using a data window of eight samples. Initially, the order estimator fills the data window and, hence, the indicated order estimate increases to 8. After this, the order estimator settles to 2, indicating that even though we attempted to excite only one mode, there were, in fact, two significant modes excited. Note also that the norm of the forward estimation error is small compared with the value at the start of the process when the order estimate was settling.

The modal amplitudes obtained from the lattice filter are spectrally decoupled, by using the aforementioned procedure, after enough data are taken to obtain the DFT accurately (for 64 time samples, about 1 sec). This occurs at about 1.75 sec, with the first 0.75 sec being used for the identification of mode shapes and model order. (See fig. 17.) Figure 17 shows the modal amplitudes for both of the identified modes. These are the signals that are inputs to the parameter-identification method used to identify the parameters of the ARMA model of the modes. The identified ARMA parameters are shown in figure 17 for each of the two modes identified. The a priori parameter estimates are initially offset from the values predicted by a finite-element analysis, which are also indicated in figure 17. These parameters track the instantaneous value required to minimize the output error. One possible explanation of the oscillatory behavior of the mode 2 parameter estimates is the nonlinearity of the actuator compensation. Nonlinearity is apparent in the sensor 6 data in figure 16. Note that the lattice filter produces a linear least-squares fit of the data to the measurements and, in so doing, produces a predominantly linear first-mode estimate and lumps the nonlinear dynamics into the higher modes. Thus, the parameter tracking is more stable in mode 1 and produces estimates of an undamped ($A_2 = -1$) os-

cillation at nearly 2.7 Hz. If the algorithm is constrained to an order estimate of 1, the predominant response is linear; however, the fit error is increased by an order of magnitude.

The mode-shape estimates obtained from the lattice filter are shown in figure 18 in which we compare the estimates obtained by three methods (one analytical and two experimental). The analytical result is the primary mode shape of the beam using the Euler-Bernoulli theory. The two experimental results, which are in substantial agreement, are the nonlinear least-squares algorithm of reference 17 and the lattice-filter algorithm of this report. Again, note that there is apparently an effect of the four attached actuators on the dynamics of the test article. The lattice filter produces two modes, one near the mode of reference 17 (mode 2 of the lattice-filter output in fig. 6) and another that is shown in figure 18. This other estimated mode does not resemble any mode analytically predicted by using the linear Euler-Bernoulli theory; rather, it can perhaps be attributed to the effect of nonlinearities in the apparatus.

Adaptive Control Simulation Results

The closed-loop adaptive control method of figure 1 has been tested in the digital simulation for the 12-ft, flexible free-free beam at the Langley Research Center. The simulation contains one rigid-body mode and the first three flexible modes. Nine deflection sensors were used for obtaining the measurement data and four actuators were employed for control purposes. The natural mode shapes and their frequencies are shown along with the sensor and actuator locations in figure 6. The initial conditions on the modal amplitudes were set to 0.05 in., and the modal velocities were set to 0. The modal damping was also set to 0. A digital sampling rate of 32 Hz was selected for the simulation, and the standard deviation for measurement noise was assumed to be 0.005, based on the noise observed in the available hardware. The lattice-filter estimates are based on a data-window size of 4 (ref. 5). The testing procedures are all carried out based on a data window NW of 10 samples. Initial parameter guesses are offset from the true values to demonstrate the rapid convergence of the identification algorithm. An arbitrary delay of 2 sec was added between the time that identification starts and the time that the control would be applied to show the behavior of the identification method.

The parameter-testing method is shown in figure 19. Note that the inputs are both modal displacements and parameter estimates. This procedure is run at each time step; and if any one test fails, no control will be applied.

At the start of the simulation, the lattice filter determines the number of modes in the simulation along with the mode shapes. Modal amplitude time histories are then generated. From the lattice-filter mode shapes and modal amplitudes, natural modes and modal amplitudes are obtained through the linear transformation. The application of the transformation is delayed for 2 sec because the on-line transformation technique of reference 3 requires 2 sec of data for a fast Fourier transform data base to obtain the required transformation. The natural modal amplitudes are input to the equation-error parameter identifier that identifies the ARMA parameters. The identification results are then tested by using the test procedures described previously. When the tests are passed, the control is turned on. Results of the simulations are presented in figures 20 to 22.

Figure 20 shows the estimated modal displacement for the first lattice-filter mode. The order-estimate plot shows that the correct order of 4 is obtained in 0.3 sec. After the parameter identification, when all the tests are passed, the control is turned on at 5.5 sec and the modes are damped. Figure 21 shows when the tests for each mode are passed and when they are failed. The result of the adaptive control on the natural modes is shown in figure 22. It is evident that when the identification is validated by passing the tests and the control is turned on, the vibration suppression is achieved. The control forces applied by the four actuators are shown in figure 23. When the modes are damped out, the lattice-filter order estimate drops from 4 to 1, indicating that the flexible modes are damped out. Although the lattice-filter order decreased, the control design order was maintained at 4 throughout the time that the period control was on. Allowing the order to vary in real time and updating the control order are topics for further studies.

The main results of the identification and the test procedures are summarized in figure 24. It shows the identified frequency parameter A_1 for the first flexible mode along with time histories of the fit error, convergence, and information plotted over the same time scale. When all the tests are passed, the corresponding pass parameter (plotted as a binary logical variable) is set to 1. The various thresholds for the tests are also marked to indicate when the tests pass. The initial estimate of A_1 is offset from the finite-element prediction by about 100 percent so that the capability of the identification method can be demonstrated. When the identifier is turned on, the estimate converges to the true value of 1.8 from 3. The thresholds indicate that the fit error test is passed first, and then the convergence test. With enough signal in the measurements, the information test is always passed. When all tests are passed at 5.5 sec, the control is turned on. This is immediately seen from the history of A_1 as it starts deviating, indicating that the dynamics are being altered. When control is fully effective, that is, when the modes are

damped out, the measurement data will contain only the noise and then the information test will fail. Also, if the parameter excursions are large, the convergence tests will also fail, indicating a failure for the binary variable (tests pass). Once this happens, the control gain updating is stopped.

Identification Studies for a Flexible Grid

In this section, the lattice-filter identification method is tested in a structure that is more complex than that of the beam. The candidate structure considered is that of a two-dimensional flexible grid. Identification results are given by using both simulation and the experimental data obtained from the laboratory apparatus.

Figure 25 shows the flexible-grid experimental apparatus currently being built at the Langley Research Center (ref. 18). The grid is a 7-ft by 10-ft planar structure made by overlaying aluminum bars of rectangular cross section. The bars are centered every foot so that there are 8 vertical and 11 horizontal bars. As shown in figure 25, the grid is suspended by cables at two locations on the top horizontal bar. The motions of the grid perpendicular to the plane of figure 25 are the ones of interest in this study. There are nine noncontacting deflection sensors mounted on a back frame that give a 9 × 1 measurement vector. The sensor data are linked to the main Control Data CYBER 175 real time computer system at the Langley Research Center so that the identification can be carried out in real time. For the experimental tests, the locations of the sensors are indicated in figure 26.

Simulation Studies

In order to carry out the simulation of the lattice-filter identification of the flexible-grid facility, a finite-element analysis of the grid was made that included the suspension cables. For this analysis, nodes were placed at each overlapping joint on the grid, at the ceiling attachment points of the cable, and at every 1/2 ft along the cable. The grid elements connecting the nodes were modeled as bending elements, whereas the cable elements were modeled as two-force members. Thus, a total of 165 elements were included in the model. Four degrees of freedom appropriate for motion normal to the plane of the grid were considered. No damping was included in the model. Thirty modes were obtained from this analysis. The frequencies of the first eight modes are listed in table I. (See ref. 18.) The first three modes are the pendulum modes, the fourth is the first bending mode, and the fifth is the first torsional mode. The first four flexible mode shapes obtained from the finite-element analysis are given in figure 27. The finite-element analysis was an iterative method to calculate mode frequencies. The ones used in simulation are

believed to be numerically accurate since the change in the eigenvalue iterate of the higher frequency mode is $0.1(10)^{-10}$ in the final iteration. The highest frequency eigenvalue iteration was $0.1565(10)^4$.

TABLE I. MODAL FREQUENCIES OBTAINED FROM FINITE-ELEMENT ANALYSIS OF GRID

Mode	Frequency, Hz
1	0.364
2	.625
3	1.398
4	2.299
5	3.07
6	4.791
7	5.933
8	6.297
9	7.337
10	10.352

A simulation was developed that accommodates the first 15 modes of the analysis, but only 4 modes were used herein for the identification study. The modes used were modes 4, 6, 7, and 8. A sampling rate of 32 Hz was simulated with a standard deviation for the measurement noise of 0.005 in., which was based on actual sensor characteristics. Modes were simulated with modal amplitude initial conditions of 0.1. The data window for order determination included eight samples. In this work, the sensor locations were chosen based on several simulations. These locations differ from those of the experimental apparatus because they were selected to maximize the effect that simulated modes have on the sensors. This was accomplished by visual examination of the simulated sensor outputs. The selected locations are indicated in figure 26, in which an asterisk is used to distinguish simulation sensor locations from experimental ones. One may expect that location 5 would be preferable to location 5*; but since some simulated modes had little input to a sensor at location 5, location 5* proved to be a better location.

Based on the entire measurement vector, the lattice-filter order estimate is shown in figure 28. Also shown in figure 28 are sensor 5* data, which are typical of the other sensors. After estimating the order, a transformation based on the discrete Fourier transform (DFT) was carried out by using 128 samples in order to obtain the natural modes; and the equation error method was used to identify associated modal frequencies and damping. The resulting (identified) modal frequencies, damping, and mode shapes are compared with those predicted (simulated) by finite-element analysis in table II. The identification of frequencies and damping are close for

TABLE II. MODE-SHAPE COMPARISON BETWEEN SIMULATED AND IDENTIFIED RESULTS

Sensor (a)	Shape of mode 4 with frequency of—		Shape of mode 6 with frequency of—		Shape of mode 7 with frequency of—		Shape of mode 8 with frequency of—	
	2.299 Hz (simulated)	2.4 Hz (identified)	4.791 Hz (simulated)	4.8 Hz (identified)	5.933 Hz (simulated)	6.0 Hz (identified)	6.3 Hz (simulated)	6.4 Hz (identified)
1*	0.29	0.30	−0.16	−0.17	0.31	0.32	0.59	0.45
2*	−.40	−.41	−.12	−.08	−.43	−.43	0	−.43
3*	.29	.30	−.16	−.18	.31	.32	−.16	.21
4*	.30	.31	.38	.37	−.06	−.06	.01	−.09
5*	−.39	−.36	−.72	−.74	.49	.49	.01	.49
6*	.30	.30	.37	.36	−.06	−.06	−.01	−.06
7*	.31	.31	−.20	−.15	−.32	−.31	.39	−.19
8*	−.39	−.38	−.26	−.29	.41	.41	0	.37
9*	.31	.31	−.20	−.14	−.32	−.31	−.39	−.38

[a] Asterisk denotes simulated sensor.

all four simulated modes. However, the mode-shape estimates agree with simulation for only three modes. One possible explanation for this is the limitation imposed by sampling rate and the number of samples used to decouple the lattice-filter modes. By sampling at 32 Hz and including 128 data points in the DFT, a frequency resolution of only 0.25 Hz is obtained. Since the expected frequency separation between modes 7 and 8 is only 0.4 Hz, good decoupling cannot be achieved.

To summarize, the lessons learned from the simulation studies are given as follows:

1. The least-squares lattice filter gives good identification of simulated modal frequencies, damping, and mode shapes in the presence of sensor noise expected in the experimental apparatus.

2. The DFT method of obtaining natural modes from the lattice modes is inaccurate if the modes happen to be closely spaced in frequency. This may be improved by adding more samples to the DFT.

3. Sensor locations should be properly selected to ensure good identification of simulated mode shapes.

Experimental Results

Experiments were conducted by using the grid apparatus described previously. The procedure for conducting the experiments was to excite the grid by using an air shaker. The shaker was capable of periodically exhausting a jet of air that impinged on the grid at sensor location 1. The frequency of the jet was adjustable from 0 to 50 Hz. The resulting grid excitation was not purely sinusoidal but was rich in harmonics. Because of the range limits of the deflection sensors (0 to approximately 2 in.), the maximum peak-to-peak deflections of the grid were limited to about 1 in. When the peak-to-peak deflection neared this limit, the air shaker was turned off and the grid was allowed to vibrate freely with only air and material damping. A CYBER 175 real time computer system sampled the deflection sensor data at 32 Hz for 5 sec. The data were stored on a system data file for further analysis. This test procedure was repeated for several shaker frequencies in the range from 1 to 10 Hz. This range has an upper limit because of the sampling frequency (32 Hz), and the lower limit is selected to include the predicted lowest vibration mode (2.2 Hz). Eight data sets corresponding to different shaker excitation frequencies were created and stored on tapes. The following discussion pertains to results extracted from data tape 5.

Figure 29 presents data from sensors 1 and 4 as well as the lattice-filter order estimate. For this case, the order estimate was based on a data window of 8 samples and spectral decoupling was done with 64 time samples. From this figure, the order estimate is seen to converge to an oscillation between 2 and 3 at about 0.5 sec. At

about 0.8 sec, the order estimate was fixed at 3 and a data collection of the 64 time samples required for the DFT was started at 32 Hz. The DFT was accomplished at about 2.8 sec, and then the decoupling transformation matrix was calculated. The modal amplitudes after this time should contain a single frequency, and the transformed mode shapes should correspond to the natural modes of the structure which were excited. In that manner, three modes were extracted from experimental data tape 5. These have frequencies near 0.5, 2.5, and 5 Hz. Table III presents the mode-shape estimates obtained from the experiment. Also presented are selected mode-shape predictions taken from finite-element analyses. The modes selected were those whose frequencies bracket the experimentally derived ones. The following discussion deals with the data from table III in order of increasing frequency.

A good comparison does not exist between either bracketing finite-element-analysis mode and the first experimental mode. Additionally, there is some bending in the experimental mode as evidenced by sensors 4, 5, and 6. The amplitude for this mode is shown in figure 30(a) along with the ARMA parameters A_1 and A_2 for the mode and their primary strip counterparts of damping and frequency. Figures 30(b) and (c) show the same information for the second and third modes, respectively. For the second mode, good agreement does exist between experiment and the finite-element results for the 3.07-Hz finite-element-analysis mode. Note, however, that the output of sensor 4 is opposite in sign and reduced in amplitude from the finite-element prediction. This means that a feedback on that sensor, based on the finite-element analysis, will be destabilizing near the 2.5-Hz frequency. The validity of this deduction can be established by examining the outputs of sensors 1 and 4 (fig. 29). According to the finite-element analysis, the 2.5-Hz content of the sensor outputs should be opposite in sign. However, they are in phase, that is, in agreement with the identification results.

Concluding Remarks

This report has presented a theory for identifying the dynamics of flexible structures. The theory has been applied to a one-dimensional beam and a two-dimensional grid structure by using both simulated and experimental data, and it was also used for the identification portion of a parameter adaptive control system. Identification is done based on the assumption of a modal representation of structural dynamics. First, by using least-squares lattice filters, an algorithm is developed for identification of the number of modes present in sensor data and for the calculation of the mode shapes. The algorithm uses the least-squares lattice filter that constructs an orthonormal basis for representing the measurement data. The basis is orthonormal in

TABLE III. MODE-SHAPE COMPARISONS BETWEEN ANALYSIS AND EXPERIMENT

Sensor	Experimental mode 1 comparisons for a frequency of—			Experimental mode 2 comparisons for a frequency of—			Experimental mode 3 comparisons for a frequency of—		
	0.364 Hz (analysis) (a)	0.5 Hz (experiment) (b)	0.625 Hz (analysis) (a)	2.299 Hz (analysis) (a)	2.5 Hz (experiment) (b)	3.07 Hz (analysis) (a)	4.791 Hz (analysis) (a)	5 Hz (experiment) (b)	5.933 Hz (analysis) (a)
1	−0.509	0.256	0.451	0.353	−0.452	−0.474	−0.359	−0.035	0.427
2	−.509	.461	0	−.254	.107	−.001	−.340	−.380	−.350
3	−.509	.656	−.451	.353	.436	.476	−.357	−.139	.425
4	−.260	.243	.409	.375	−.080	.133	.220	.176	−.074
5	−.260	−.09	0	−.249	.05	0	.243	.104	.072
6	−.260	.405	−.409	.375	−.030	−.133	.219	−.010	−.073
7	−.078	.098	.360	.375	.536	.505	·−.376	−.646	−.446
8	−.077	.199	0	−.244	−.068	0	−.434	.291	.318
9	−.078	.090	−.360	.375	−.540	−.507	−.375	−.539	−.443

[a] Prediction based on finite-element analysis.
[b] Calculation based on identification from experimental data.

the space of the data and not in the physical coordinate space of the structure. Hence, a transformation is developed to obtain "natural" modes from lattice-filter modes.

After obtaining the natural modes, the sensor data are processed to obtain the modal amplitude time series and an autoregressive, moving-average model is used to represent the dynamics of each mode. The coefficients of this model are the difference-equation counterparts of modal frequency, damping, and control effectiveness of actuators. The coefficients of this model are identified by using an algorithm for equation error identification. Based on these identified coefficients, a modal pole-placement control law is used to calculate the controller gains for an adaptive control method for flexible structures. Before the identification results are used for control-law design, they are validated first by a series of test procedures and the controller gains are updated only when all tests are passed.

Based on the simulation studies of the flexible beam and the grid structure, the lattice filter has been shown to provide a good on-line method for identifying the number of modes excited, mode shapes, modal damping, and modal frequencies. The results from experimental data on both the beam and the grid differ substantially from the finite-element-analysis prediction of the structural dynamics characteristics. The results indicate that reliance on finite-element analysis without ground testing may pose a problem and thus highlight the need for adaptive control or on-orbit testing.

Simulation results on adaptive control of the beam indicate that the lattice-filter identification method along with validation procedures can provide a good on-line model for control-law design and that the adaptive control can be effectively used for structural dynamics systems. This study also indicates that the lattice method can be used for both identification and control in a single algorithm that sequentially accomplishes identification followed by closed-loop control.

Langley Research Center
National Aeronautics and Space Administration
Hampton, VA 23665
July 11, 1984

References

1. Johnson, C. Richard, Jr.; and Montgomery, Raymond C.: A Distributed System Adaptive Control Strategy. *IEEE Trans. Aerosp & Electron. Syst.*, vol. AES-15, no. 5, Sept. 1979, pp. 601–612.

2. Hamza, M. H.; and Sheirah, M. A.: A Self-Tuning Regulator for Distributed Parameter Systems. *Automatica*, vol. 14, no. 5, Sept. 1978, pp. 453–463.

3. Montgomery, R. C.; and Thau, F. J.: Adaptive and Learning Control of Large Space Structures. *A Collection of Technical Papers—AIAA Guidance and Control Conference*, Aug. 1980, pp. 154–162. (Available as AIAA-80-1739.)

4. Mendel, J. M.: *Feasiblity and Design Study of Adaptive Control of Flexible, Highly Variable Spacecraft.* NASA CR-111781, 1970.

5. Sundararajan, N.; and Montgomery, R. C.: Identification of Structural Dynamics System Using Least-Square Lattice Filters. *J. Guid., Control and Dyn.*, vol. 6, no. 5, Sept.–Oct. 1983, pp. 374–381.

6. Williams, Jeffrey P.; and Montgomery, Raymond C.: Simulation and Testing of Digital Control on a Flexible Beam. *A Collection of Technical Papers—AIAA Guidance and Control Conference*, Aug. 1982, pp. 403–409. (Available as AIAA-82-1569.)

7. Sundararajan, N.; and Montgomery, R. C.: Decoupling the Structural Modes Estimated Using Recursive Lattice Filters. *Proceedings of the 21st IEEE Conference on Decision & Control*, Volume 3, 82CH1788-9, Dec. 1982, pp. 998–999.

8. Mendel, Jerry M.: *Discrete Techniques of Parameter Estimation—The Equation Error Formulation.* Marcel Dekker, Inc., 1973.

9. Lee, Daniel T. L.; Morf, Martin; and Friedlander, Benjamin: Recursive Least Squares Ladder Estimation Algorithms. *IEEE Trans. Acoust., Speech, & Signal Process.*, vol. ASSP-29, no. 3, June 1981, pp. 627–641.

10. Friedlander, Benjamin: Lattice Filters for Adaptive Processing. *Proc. IEEE*, vol. 70, no. 8, Aug. 1982, pp. 829–867.

11. Sage, Andrew P.; and Melsa, James L.: *Estimation Theory With Applications to Communications and Control.* McGraw-Hill, Inc., c.1971.

12. Montgomery, Raymond C.; and Caglayan, Alper K.: Failure Accommodation in Digital Flight Control Systems by Bayesian Decision Theory. *J. Aircr.*, vol. 13, no. 2, Feb. 1976, pp. 69–75.

13. Beneveniste, Albert; and Chaure, Christian: AR and ARMA Identification Algorithms of Levinson Type: An Innovations Approach. *IEEE Trans. Autom. Control*, vol. AC-26, no. 6, Dec. 1981, pp. 1243–1261.

14. Thau, F. E.; Montgomery, R. C.; and Horner, G. C.: On-Line Structural Parameter Identification. *A Collection of Technical Papers—AIAA Guidance and Control Conference*, Aug. 1981, pp. 530–539. (Available as AIAA-81-1846.)

15. Sundararajan, N.; and Montgomery, R. C.: Experiments Using Least Square Lattice Filters for the Identification of Structural Dynamics. *A Collection*

of Technical Papers—AIAA/ASME/ASCE/AHS 24th Structures, Structural Dynamics and Materials Conference, Part 2, May 1983, pp. 206–210. (Available as AIAA-83-0880.)

16. Montgomery, Raymond C.; Horner, Garnett C.; and Cole, Stanley R.: Experimental Research on Structural Dynamics and Control. *Dynamics and Control of Large Flexible Spacecraft—Proceedings of the Third VPI & SU/AIAA Symposium*, L. Meirovitch, ed., June 1981, pp. 365–372.

17. Thau, F. E.; Eliazov, T.; and Montgomery, R. C.: Least-Squares Sequential Parameter and State Esti-

mation for Large Space Structures. *Proceedings of the 1982 American Control Conference*, 82CH1772-3, American Automatic Control Council, June 1982, pp. 16–21.

18. Horner, Garnett C.: Optimum Actuator Placement, Gain, and Number for a Two-Dimensional Grillage. *A Collection of Technical Papers—AIAA/ASME/ASCE/AHS 24th Structures, Structural Dynamics and Materials Conference*, Part 2, May 1983, pp. 179–184. (Available as AIAA-83-0854.)
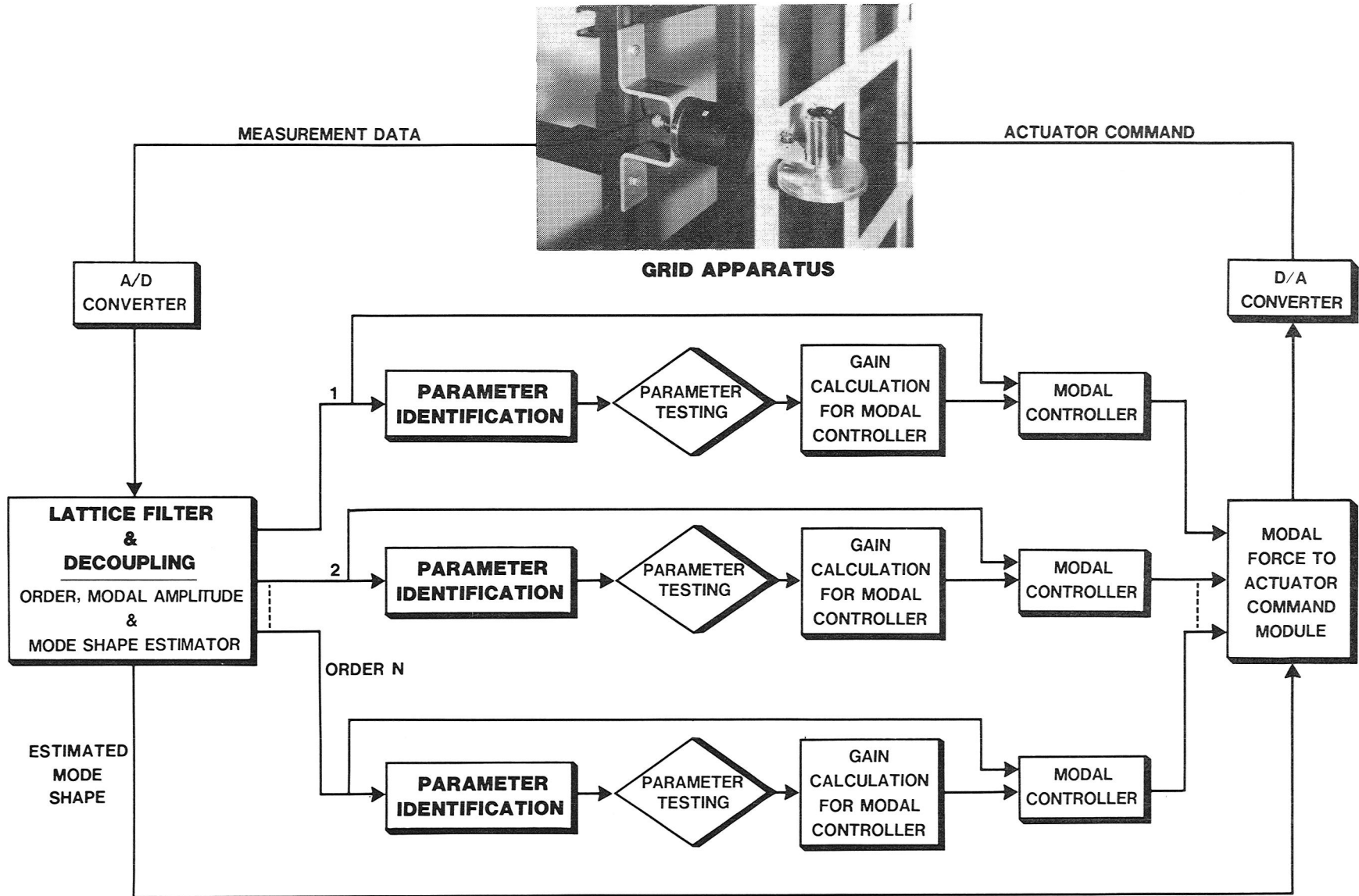
Figure 1. Distributed adaptive control using lattice-filter identification.

L-84-9443

$$r_{i,n} = y_{i-n} - \mathcal{E}(y_{i-n}|Y_i^n)$$

$$e_{i,n} = y_i - \mathcal{E}(y_i|Y_{i-1}^n)$$
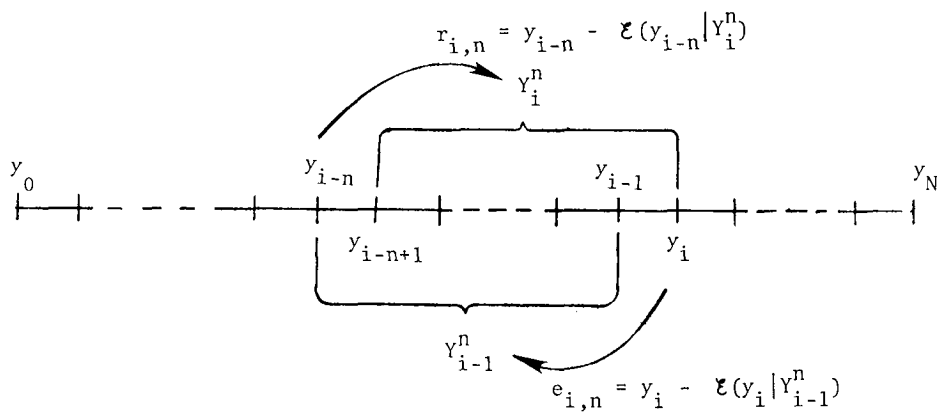
Figure 2. Schematic diagram ordering the measurement sequence.

$$\hat{y}_N^n = \mathcal{E}(y_N|Y_{N-1}^n)$$

$$\hat{y}_N^2 = \mathcal{E}(y_N|Y_{N-1}^2)$$

$$\hat{y}_N^1 = \mathcal{E}(y_N|Y_{N-1}^1) = \mathcal{E}(y_N|Y_{N-1})$$

$$\hat{y}_N^0 = 0$$
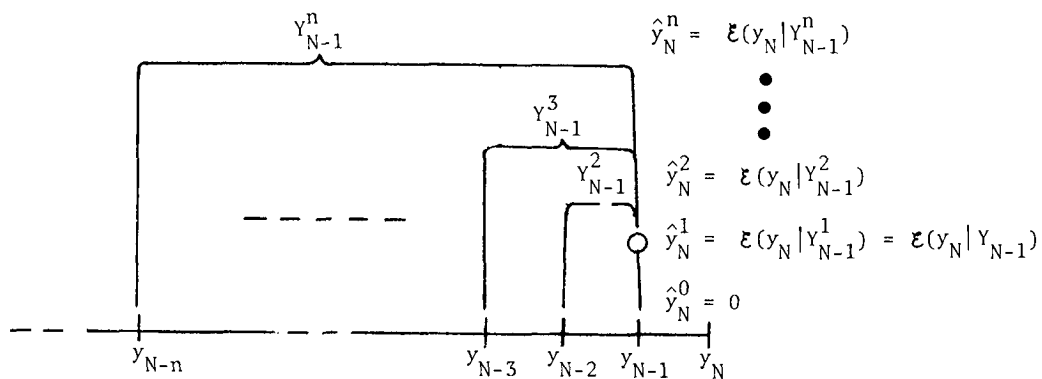
Figure 3. Nesting of estimation.

$$k = k_{i,n+1} = \langle \underline{e}_{i,n}, \underline{r}_{i-1,n} \rangle$$
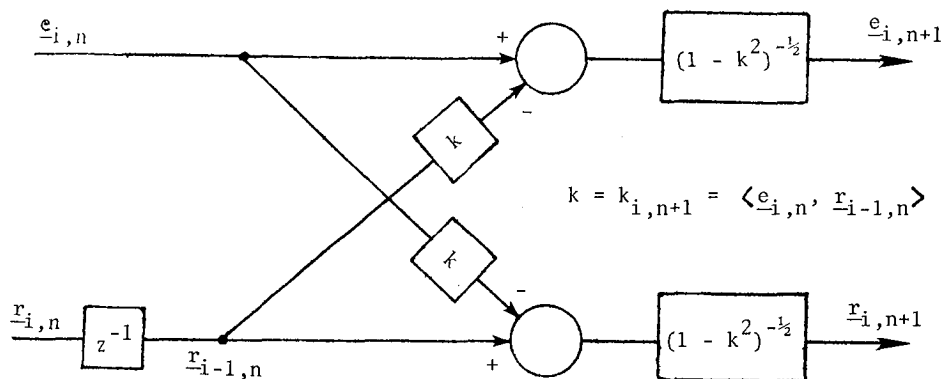
Figure 4. Flow diagram of a lattice section.
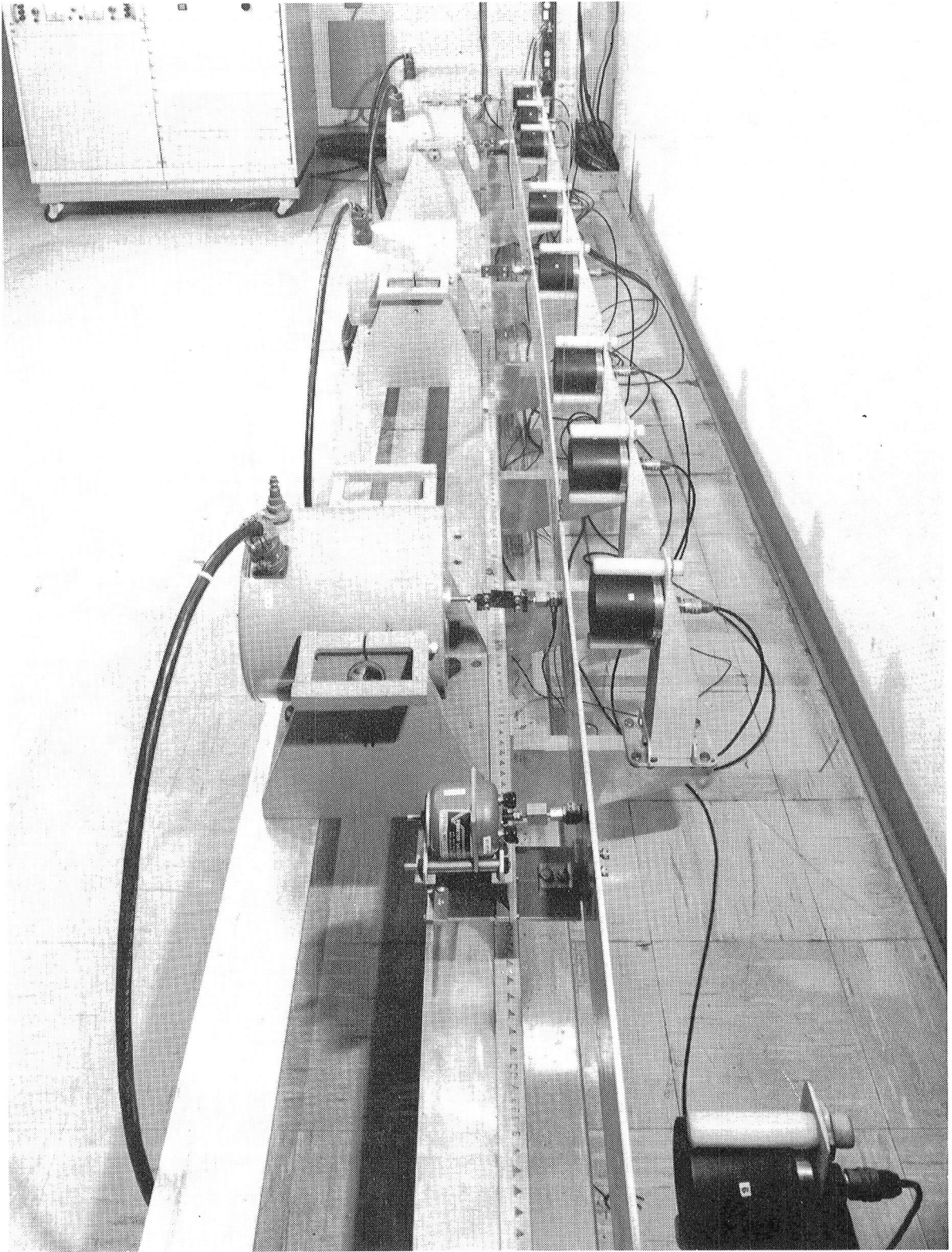
L-80-8918

Figure 5. Photograph of beam apparatus.
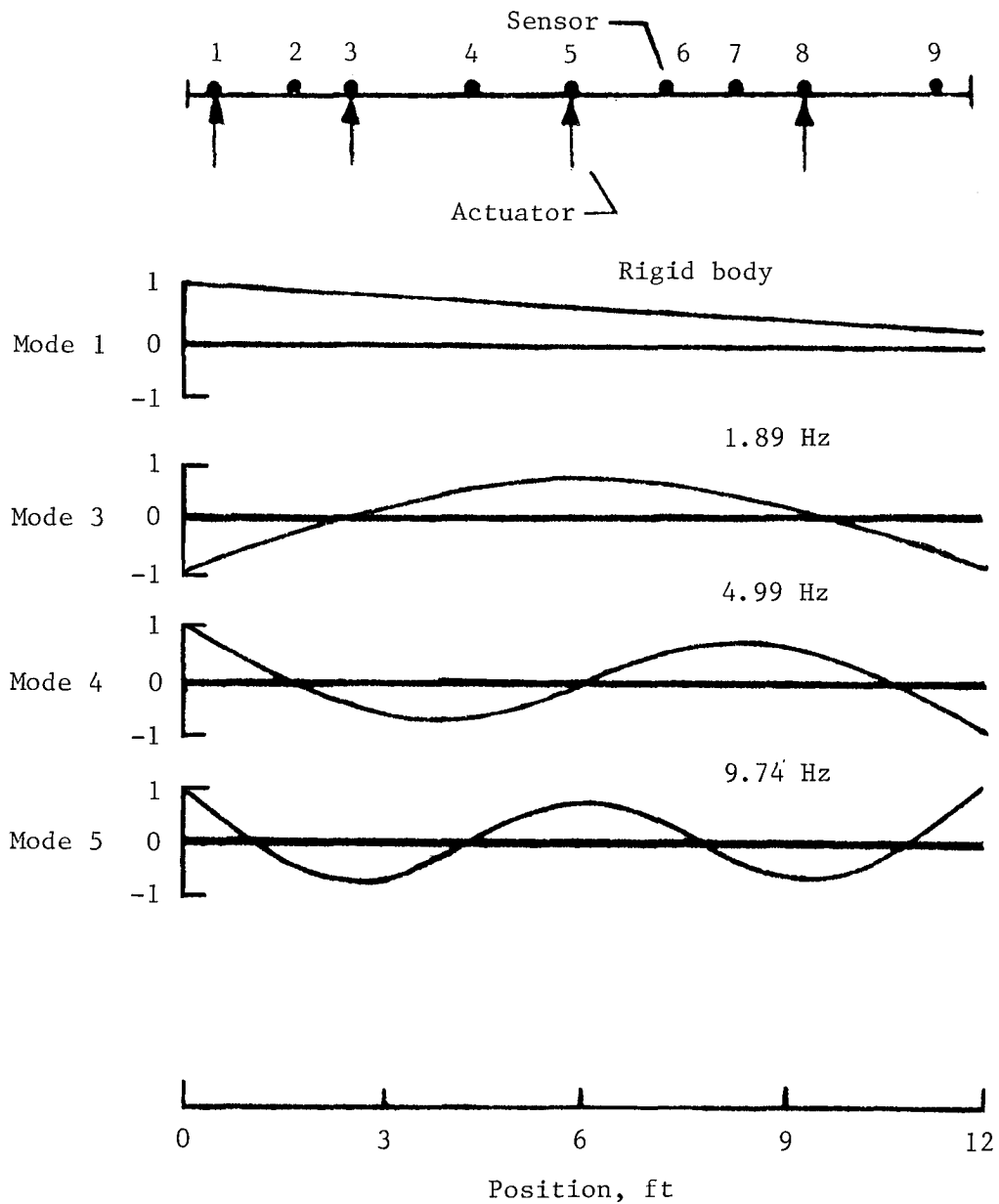
Figure 6. Natural mode shapes and their frequencies along with sensor and actuator locations.
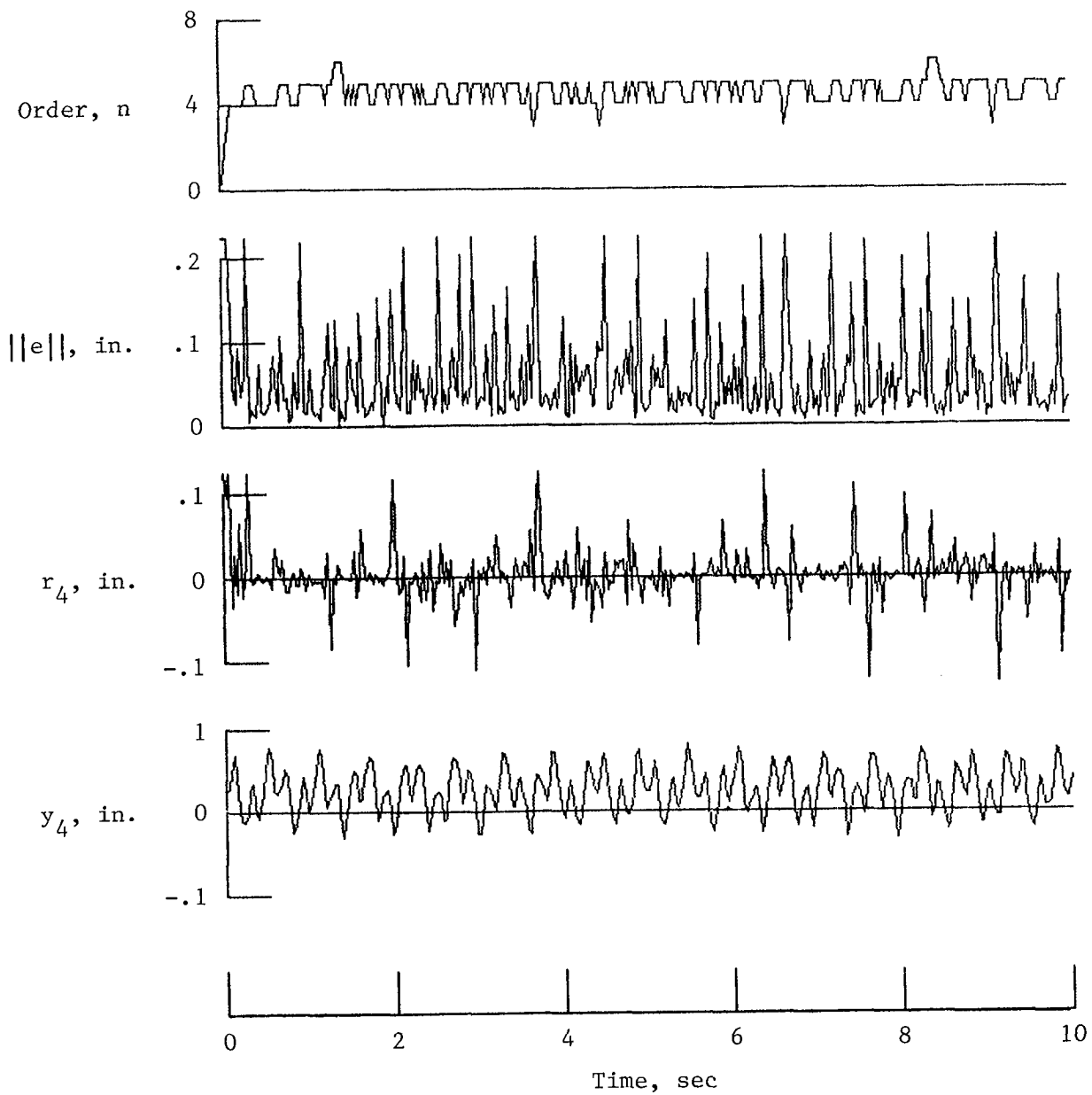
Figure 7. Simulation results for nominal case.
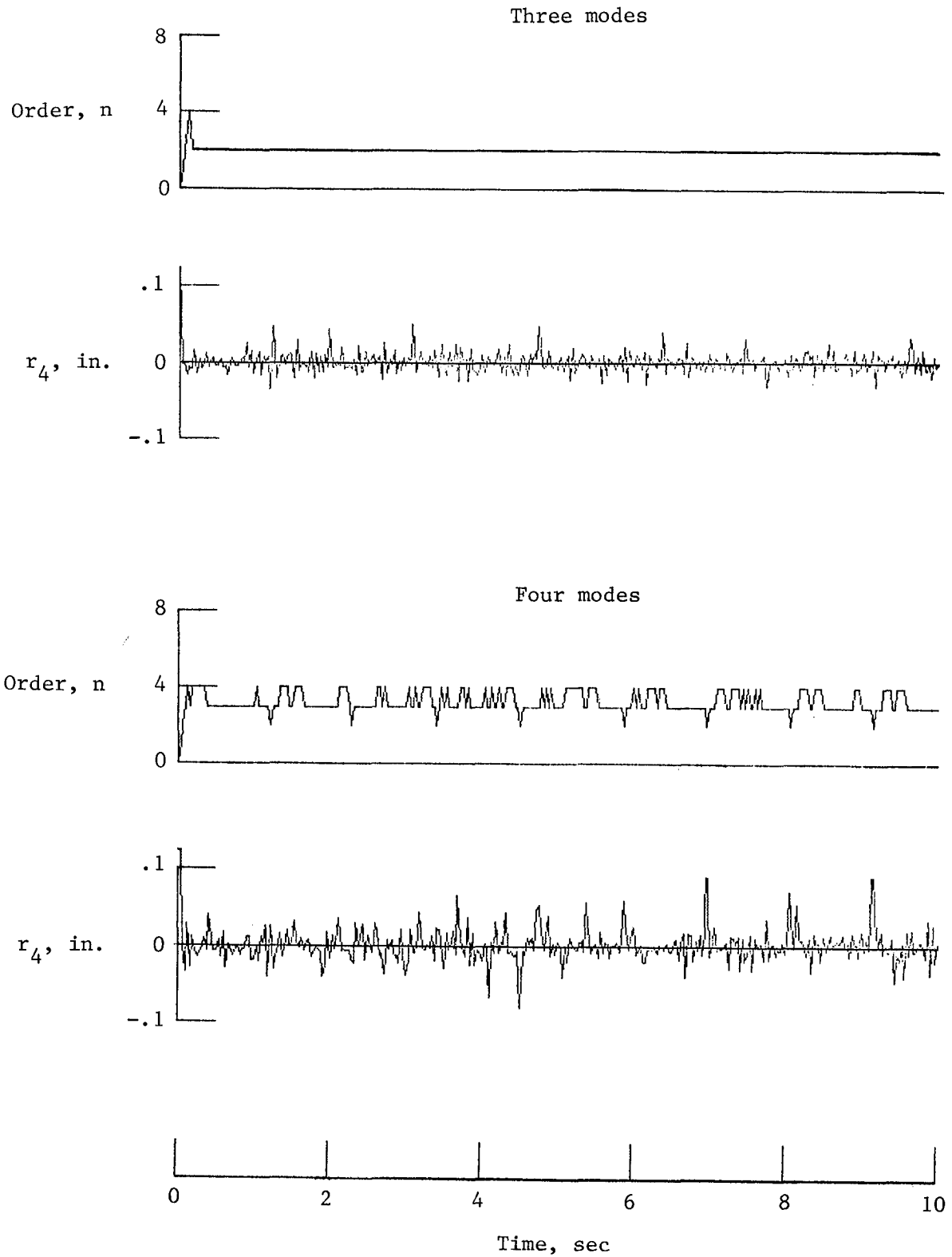
Figure 8. Comparison of cases with three and four modes.
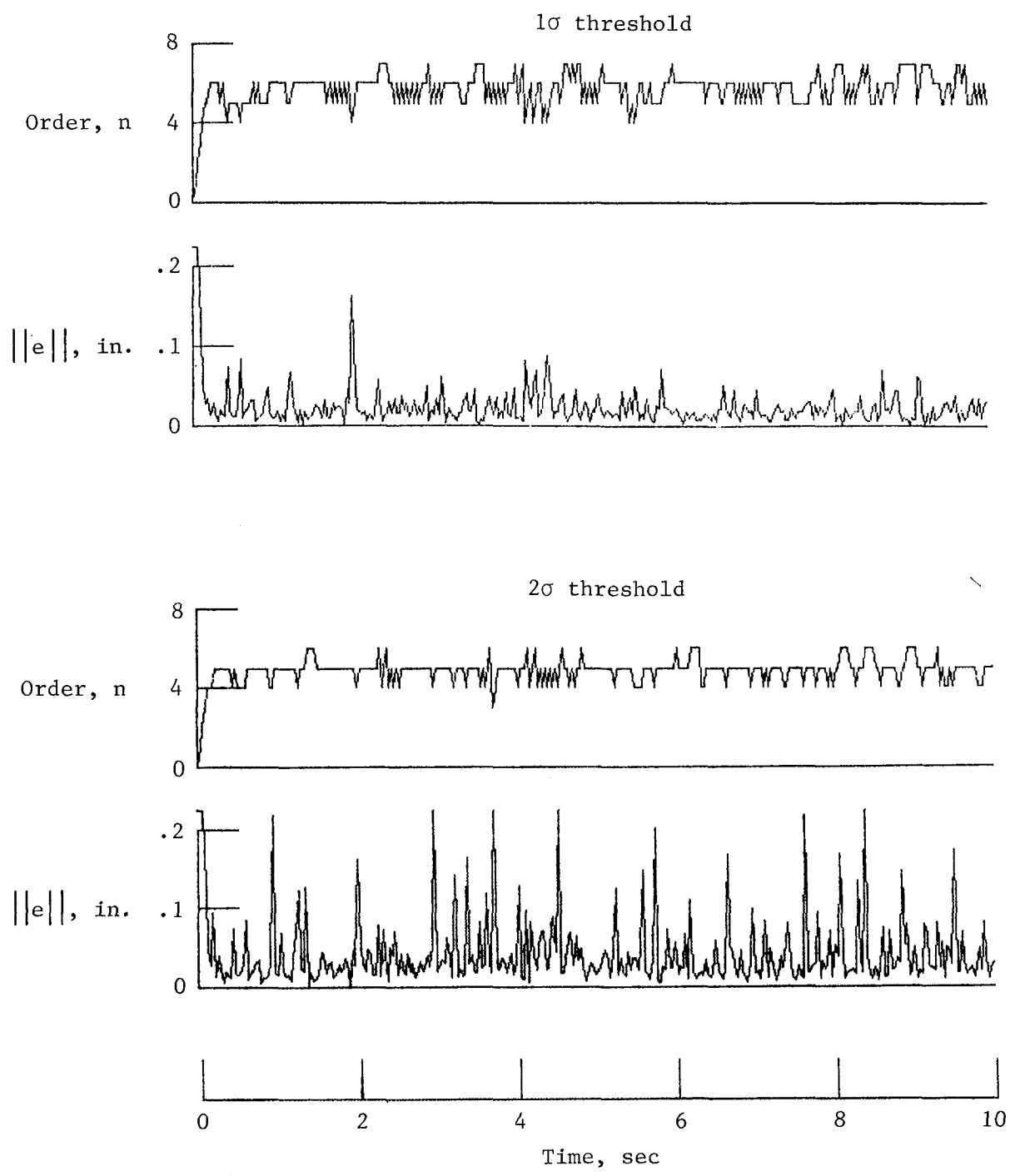
Figure 9. Effects of threshold on order determination.
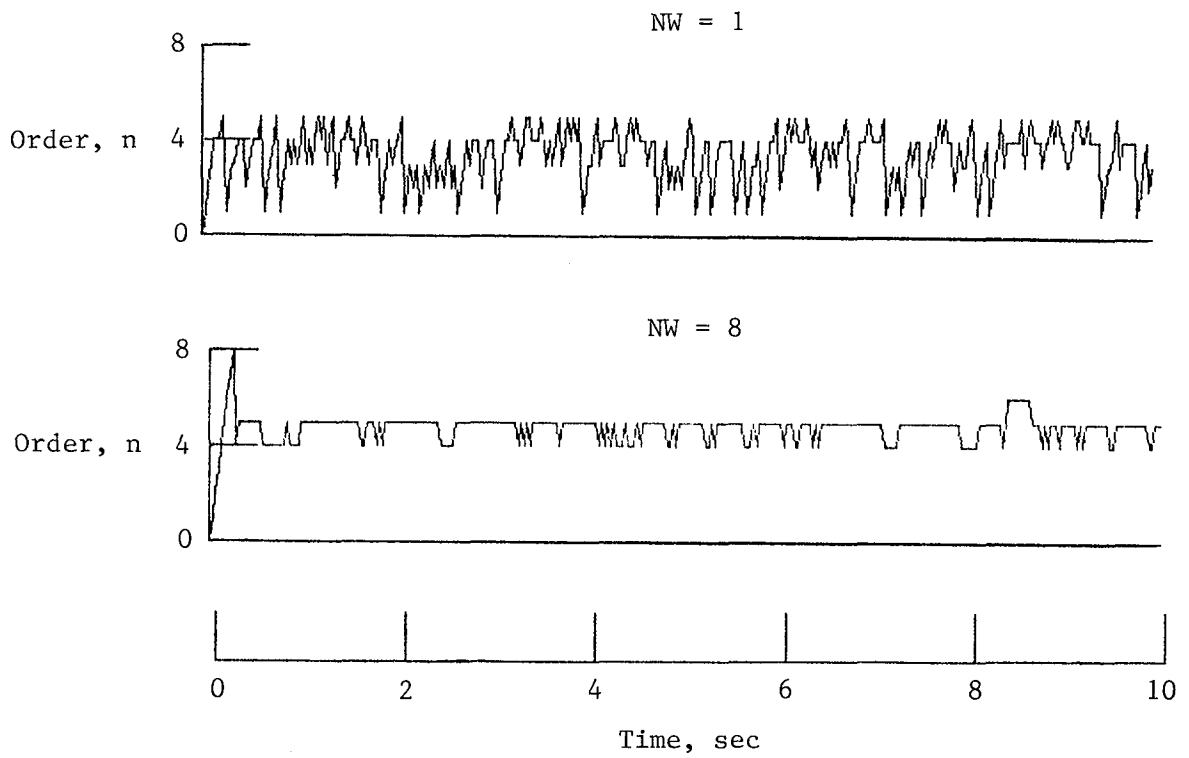
Figure 10. Effects of data-window size on order determination.
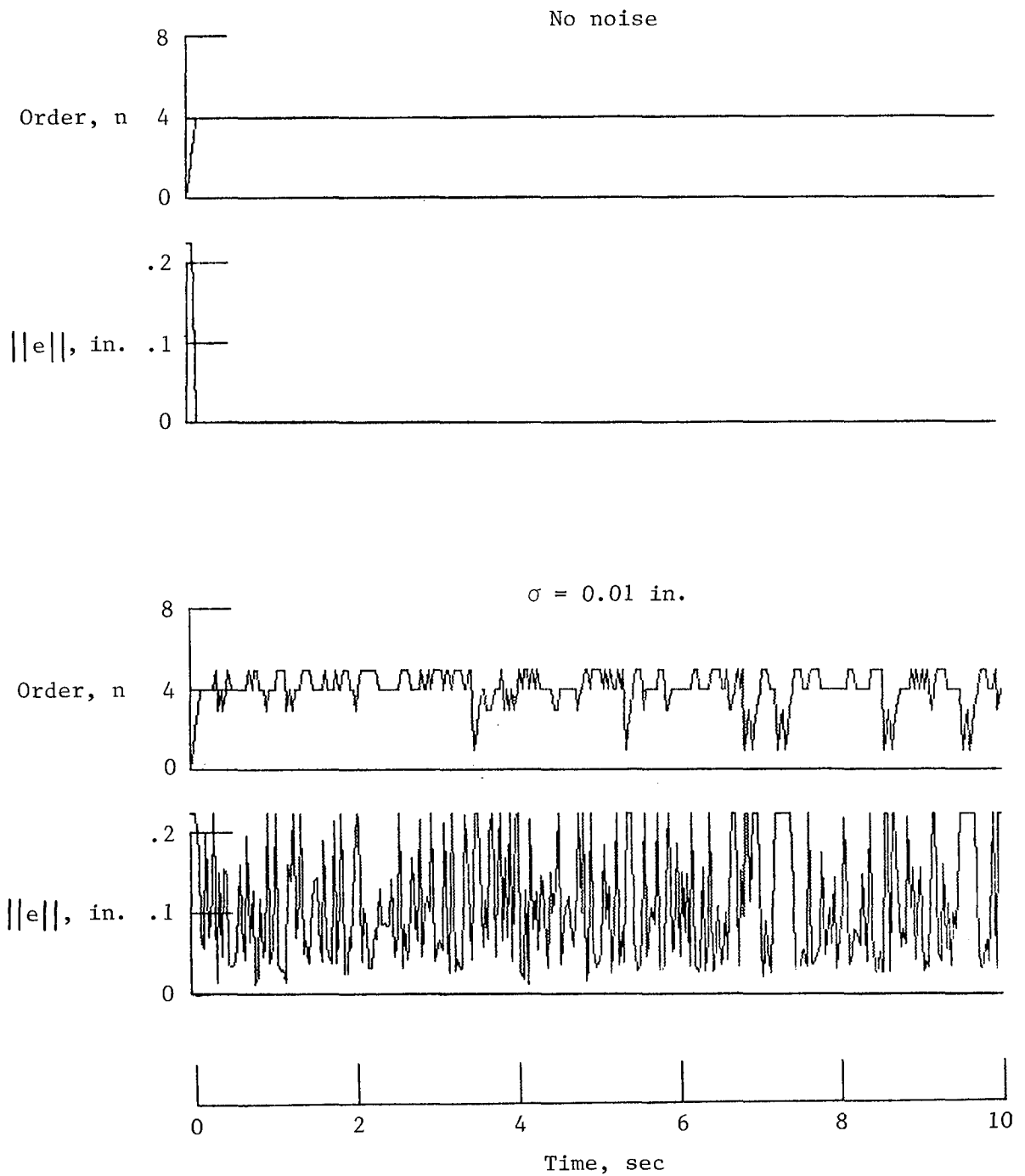
Figure 11. Effects of additive sensor noise on order determination.
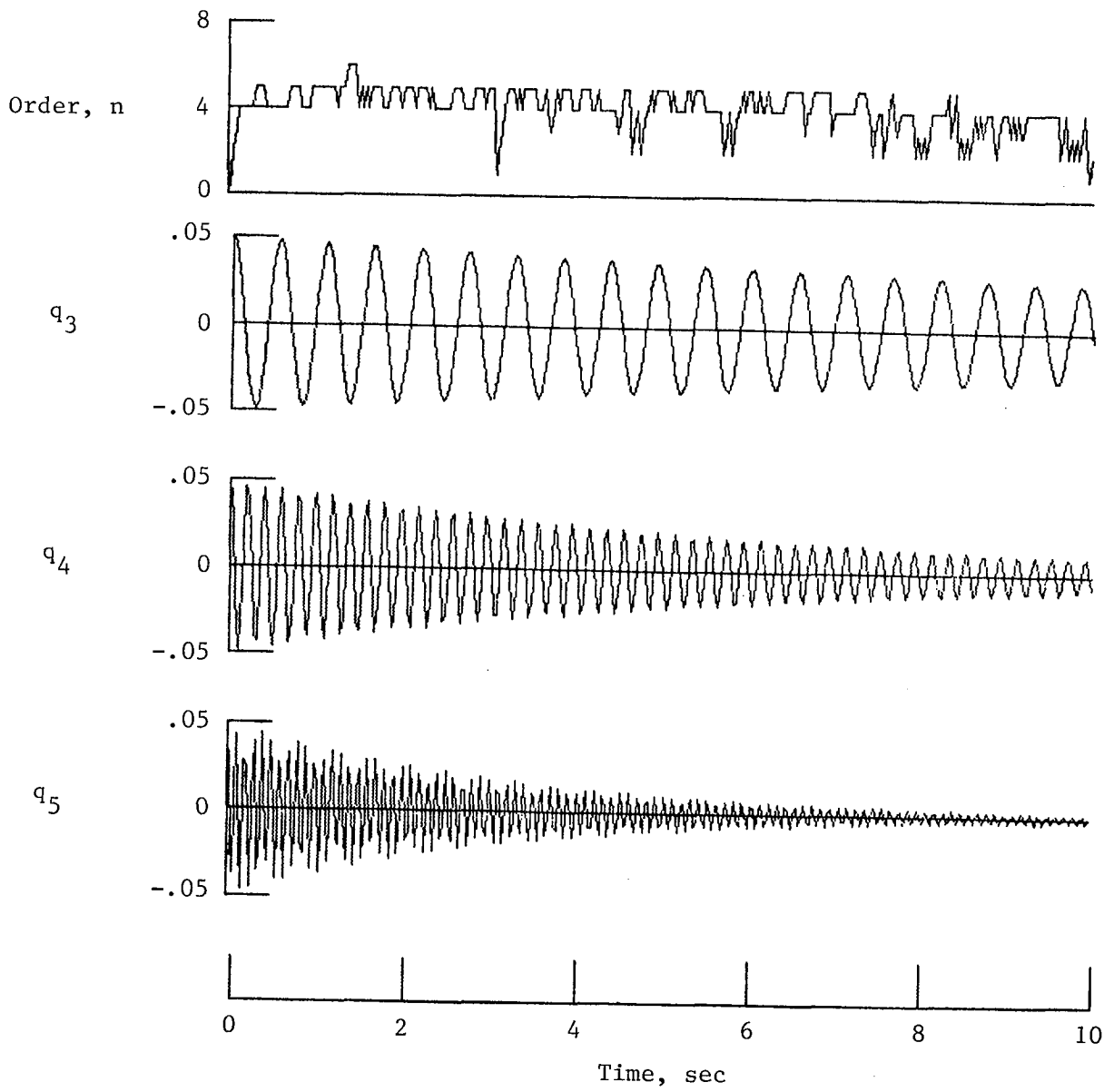
Figure 12. Effects of damping on order determination.
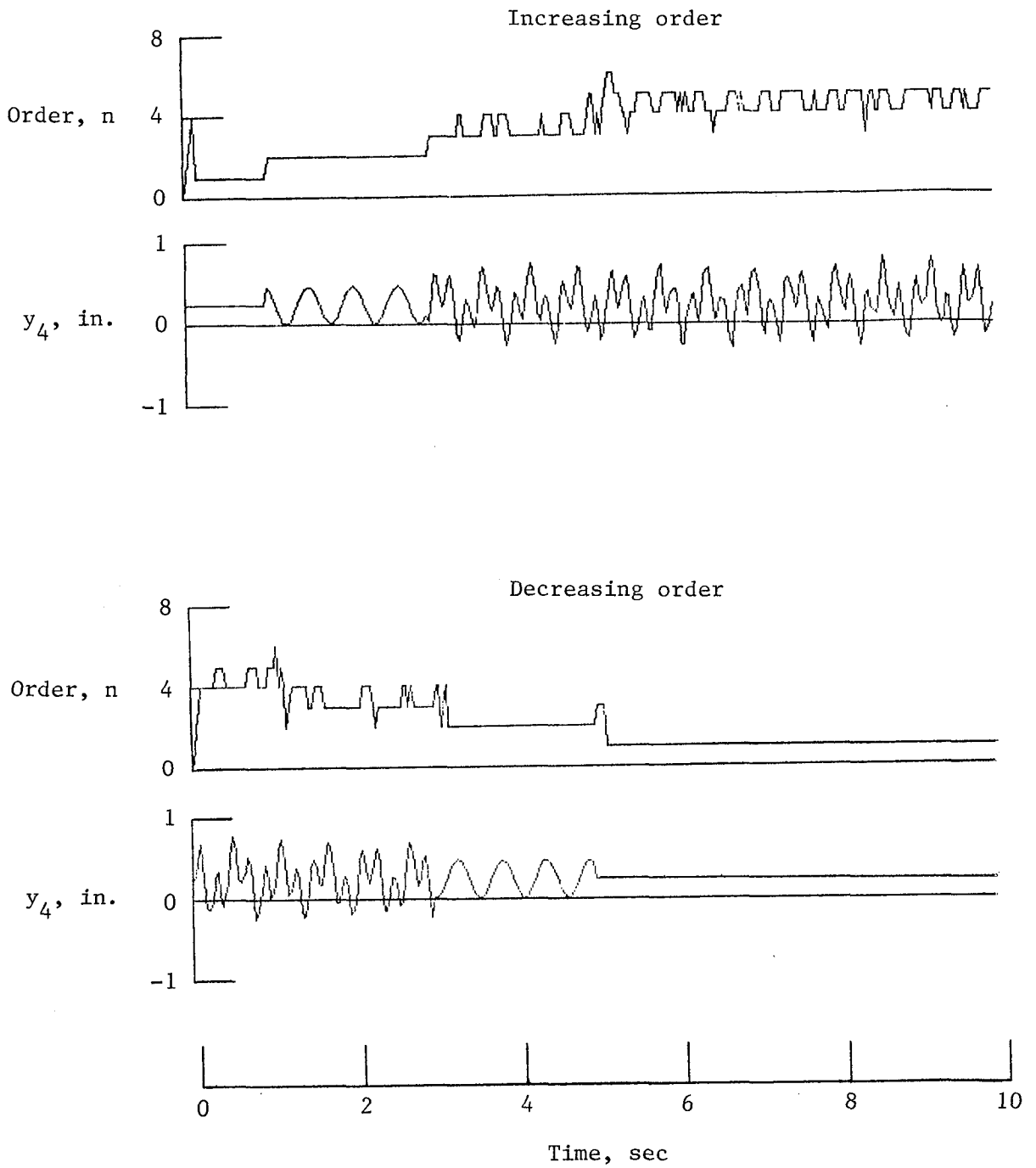
Figure 13. Model order tracking.
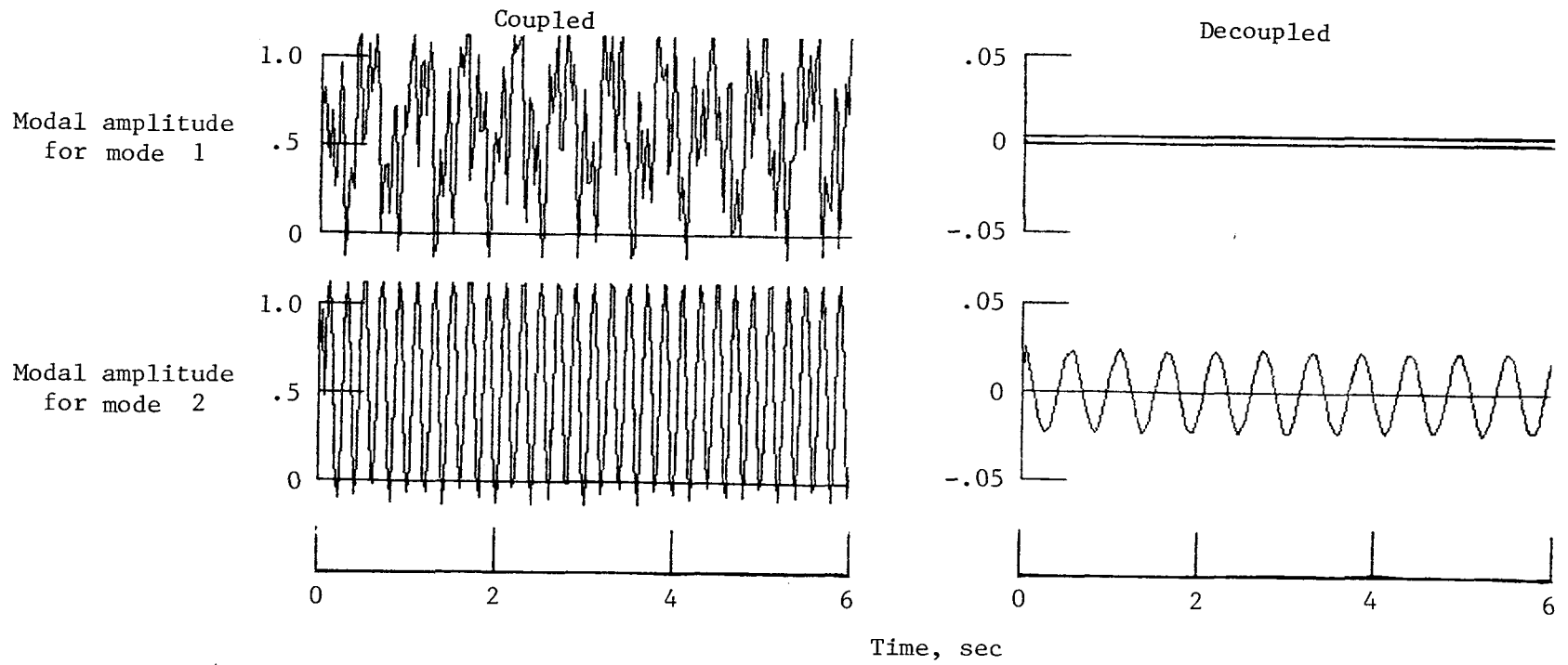
Figure 14. Comparison of coupled and decoupled modal amplitude time histories.
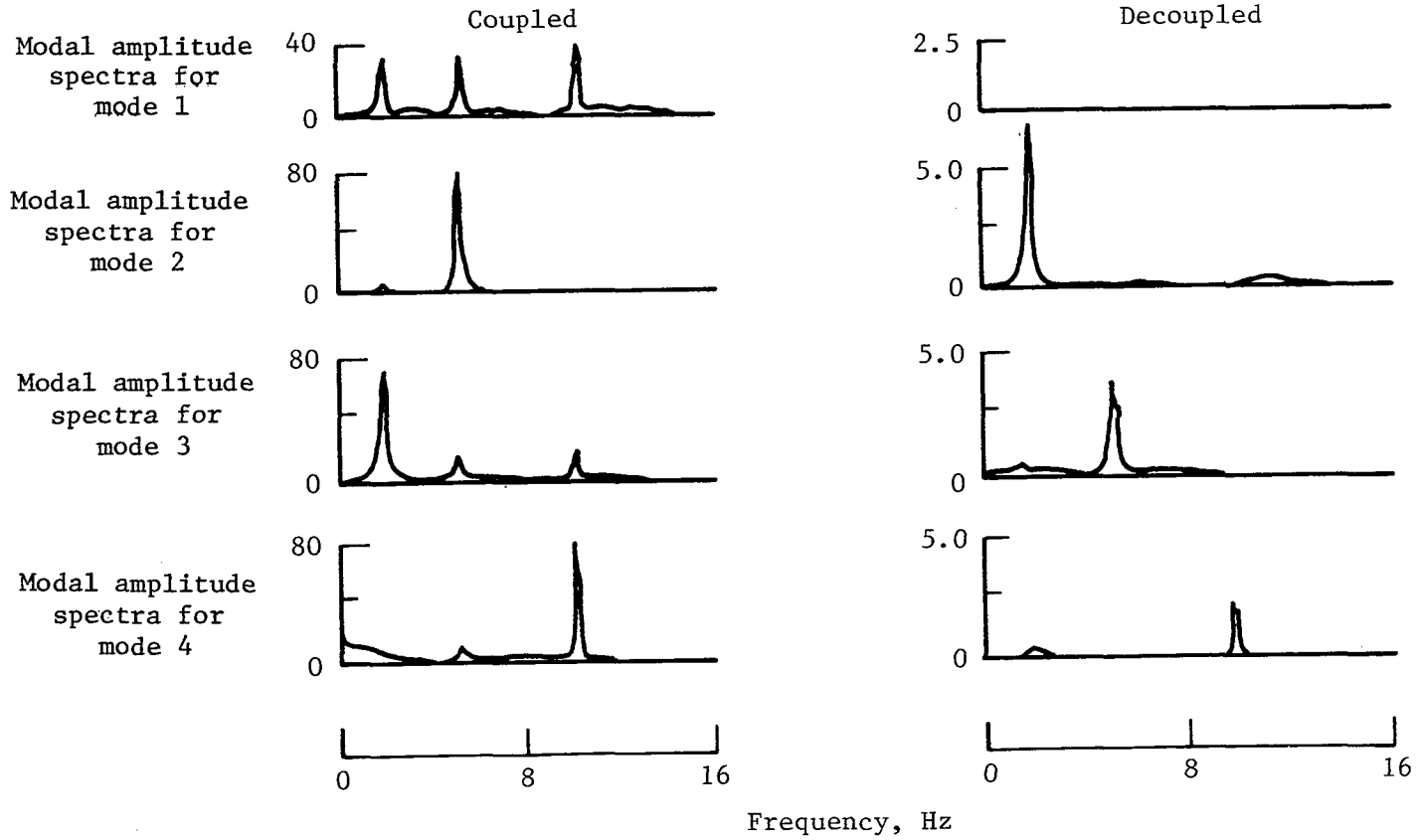
Figure 15. Comparison of coupled and decoupled modal amplitude spectra.
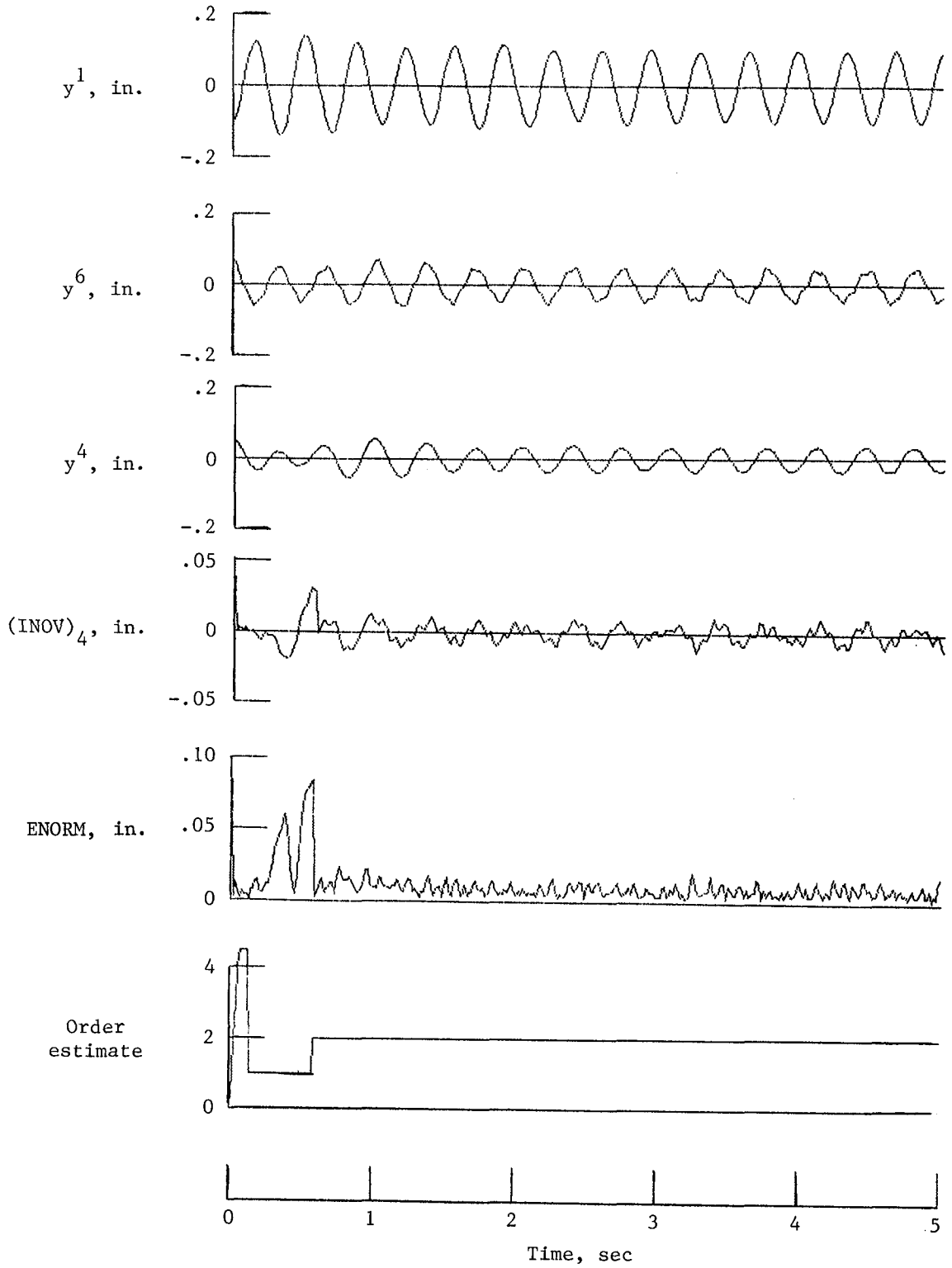
Figure 16.- Data relevant to real-time processing of algorithm.
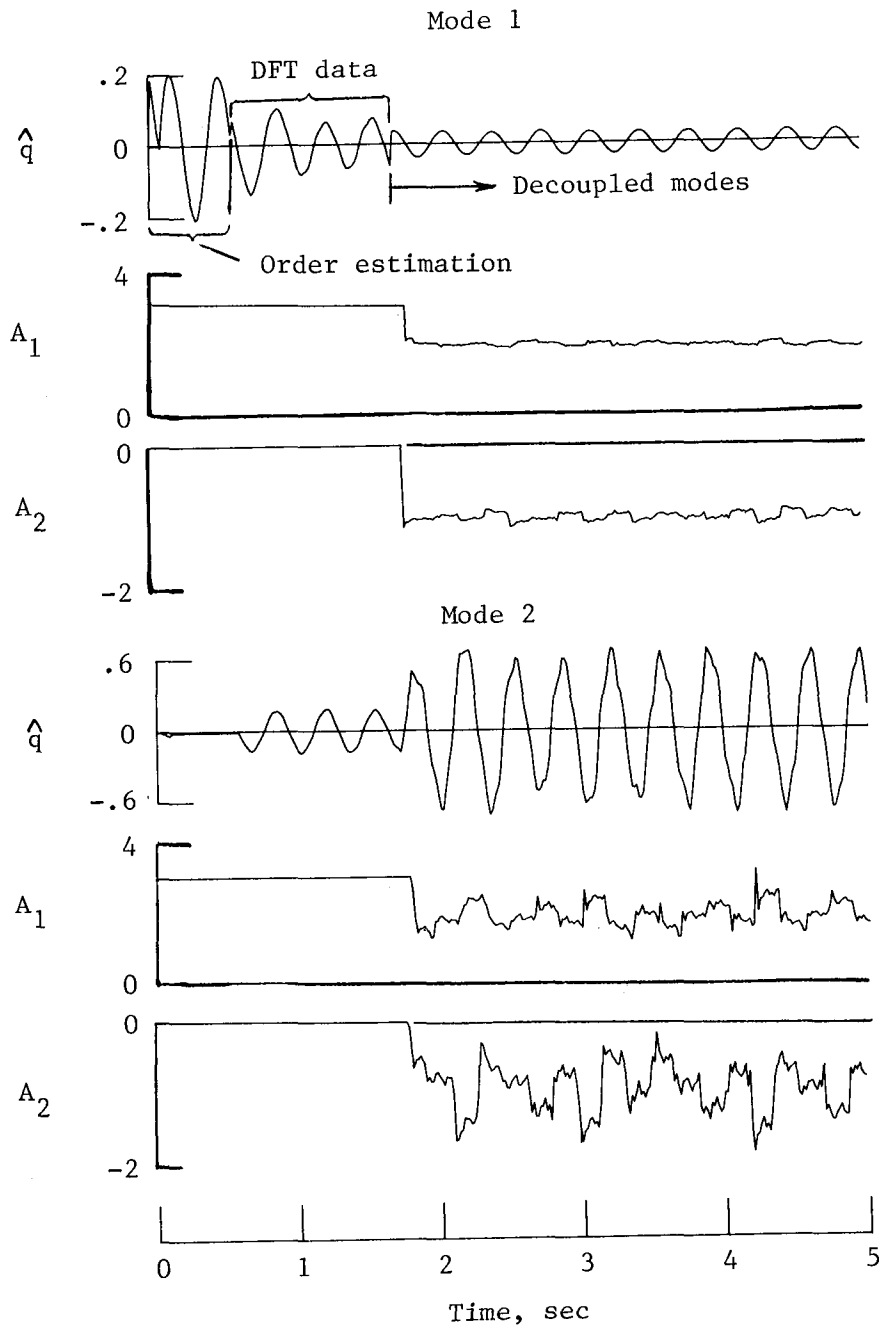
Figure 17. Estimated modal amplitudes and identified ARMA parameters resulting from algorithm.
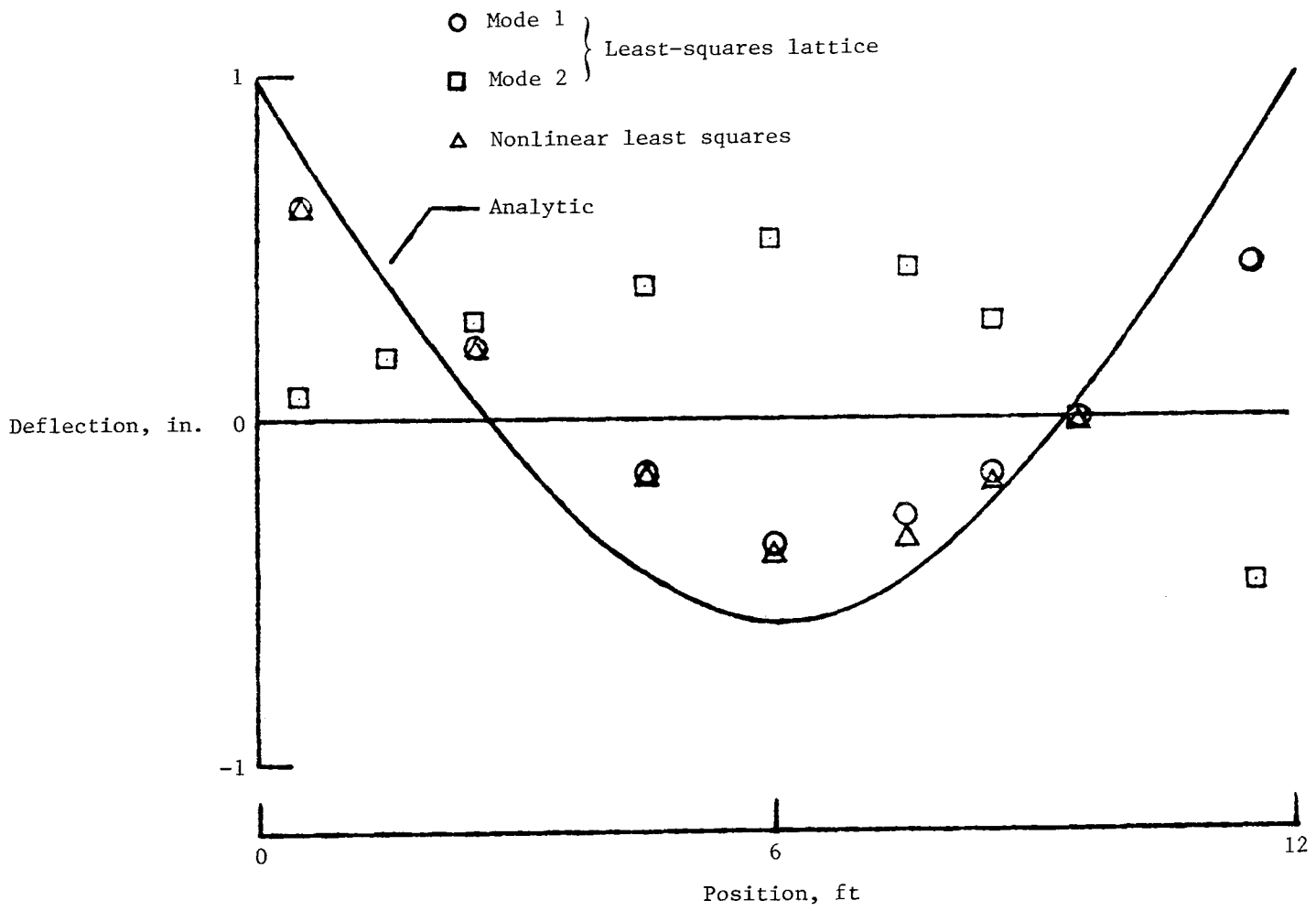
Figure 18. Mode-shape estimates obtained from the algorithm and a comparison with an analytic prediction and the estimates obtained by using the nonlinear least-squares technique of reference 15.
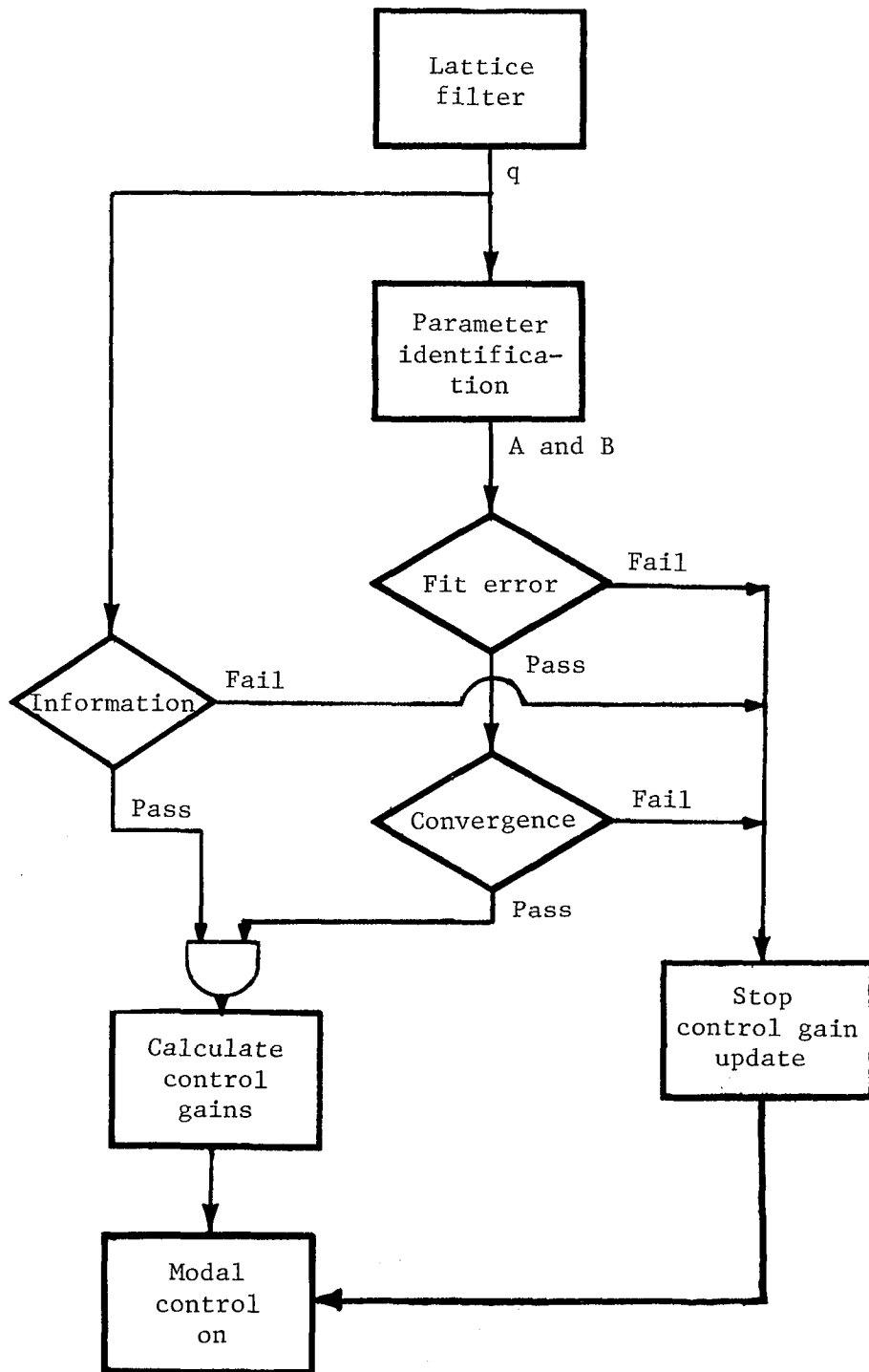
Figure 19. Flow diagram for adaptive control parameter testing.
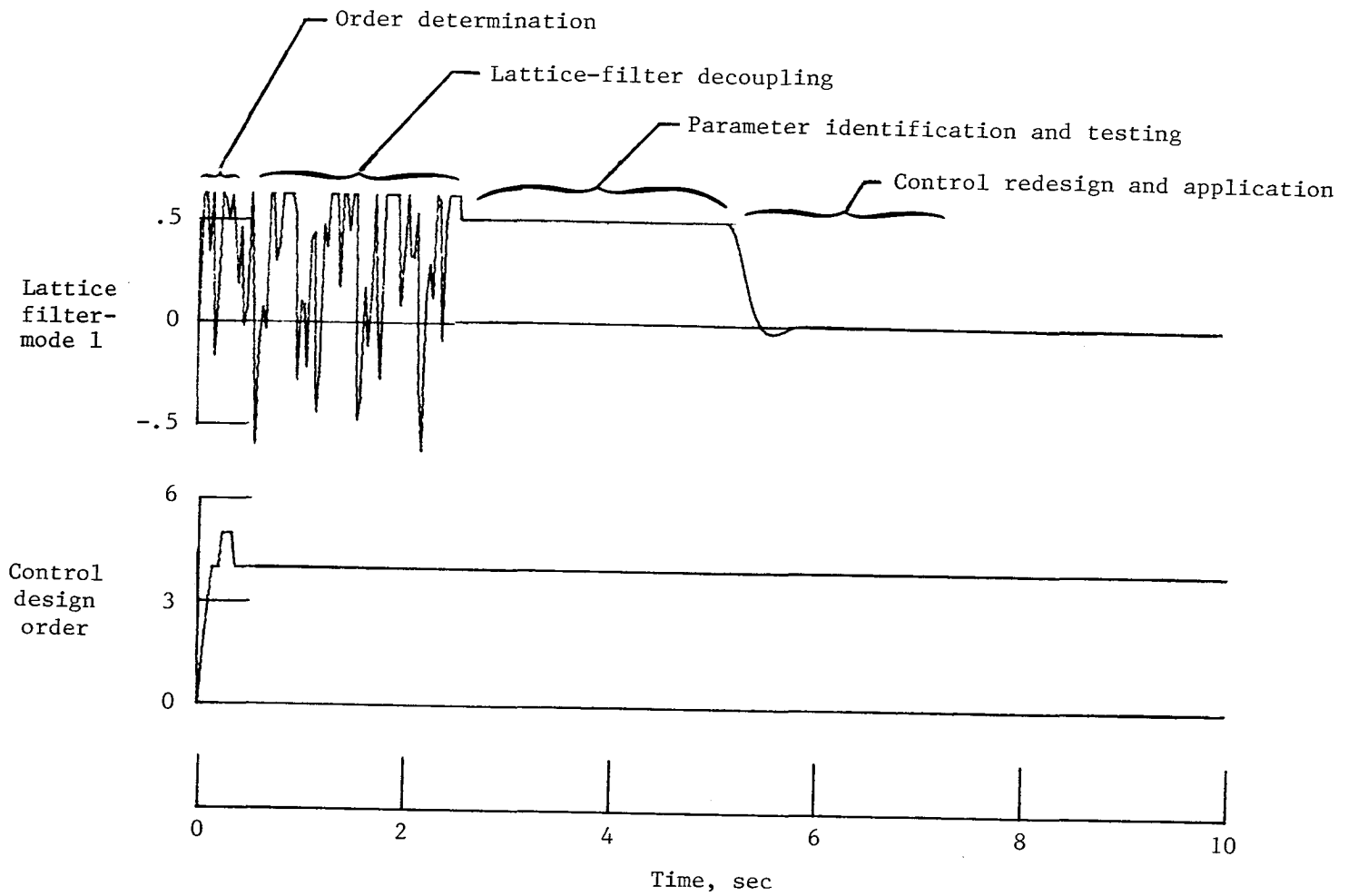
Figure 20. Typical time history of an adaptive control run using on-line identification, testing, and control design.
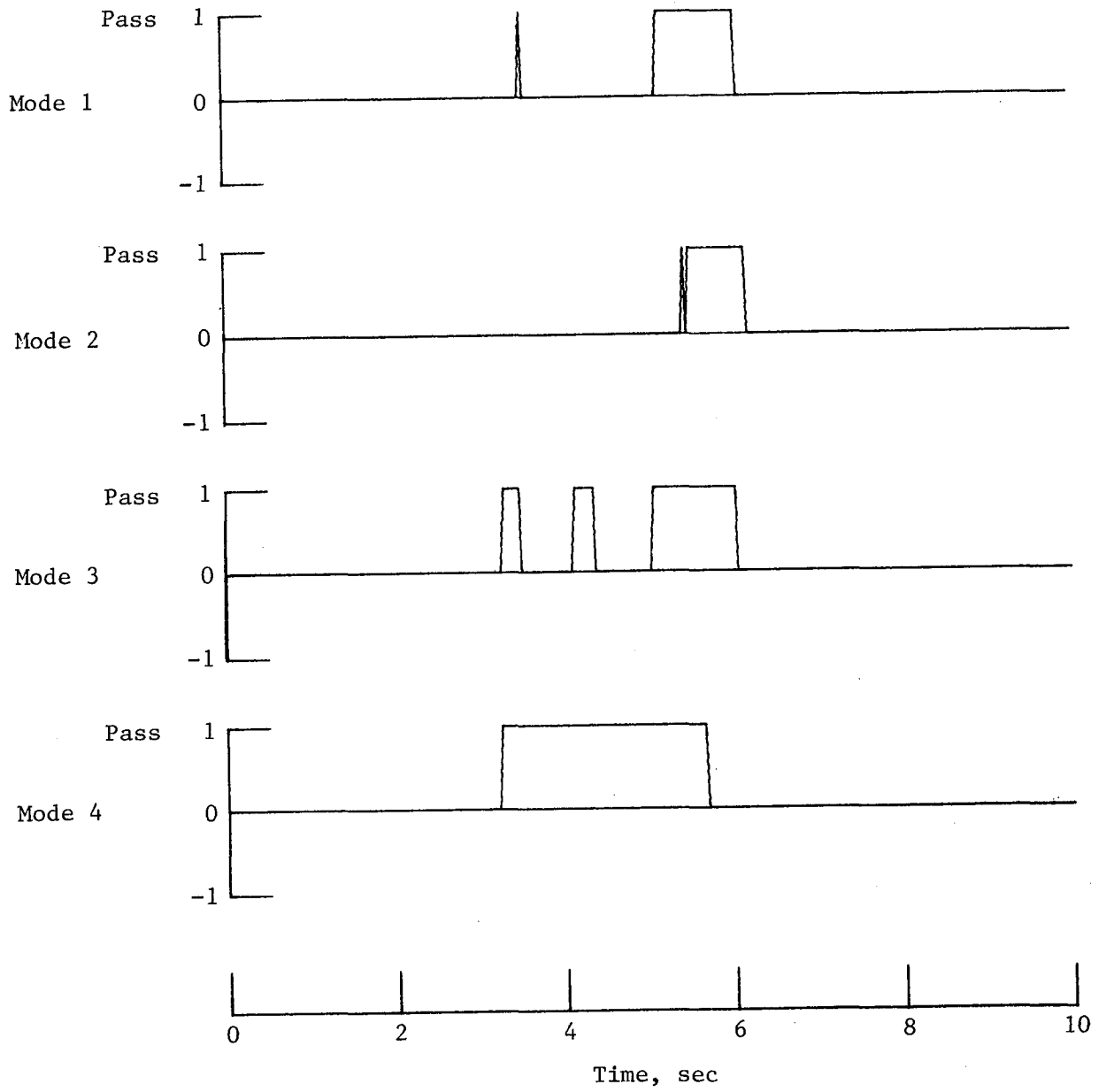
Figure 21. Test status for each controlled mode.
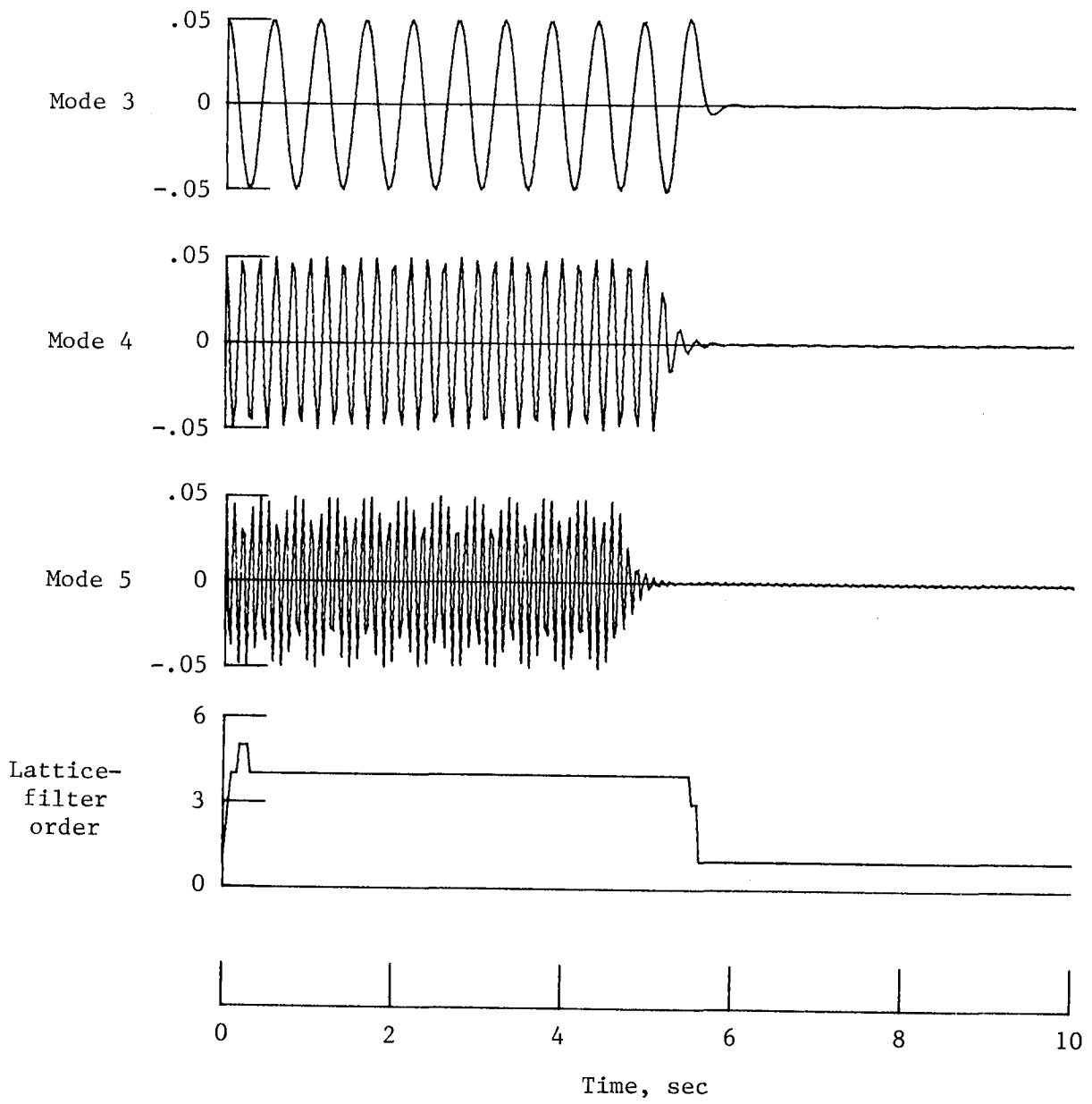
Figure 22. Time histories of three natural modes with lattice-filter order indicated.
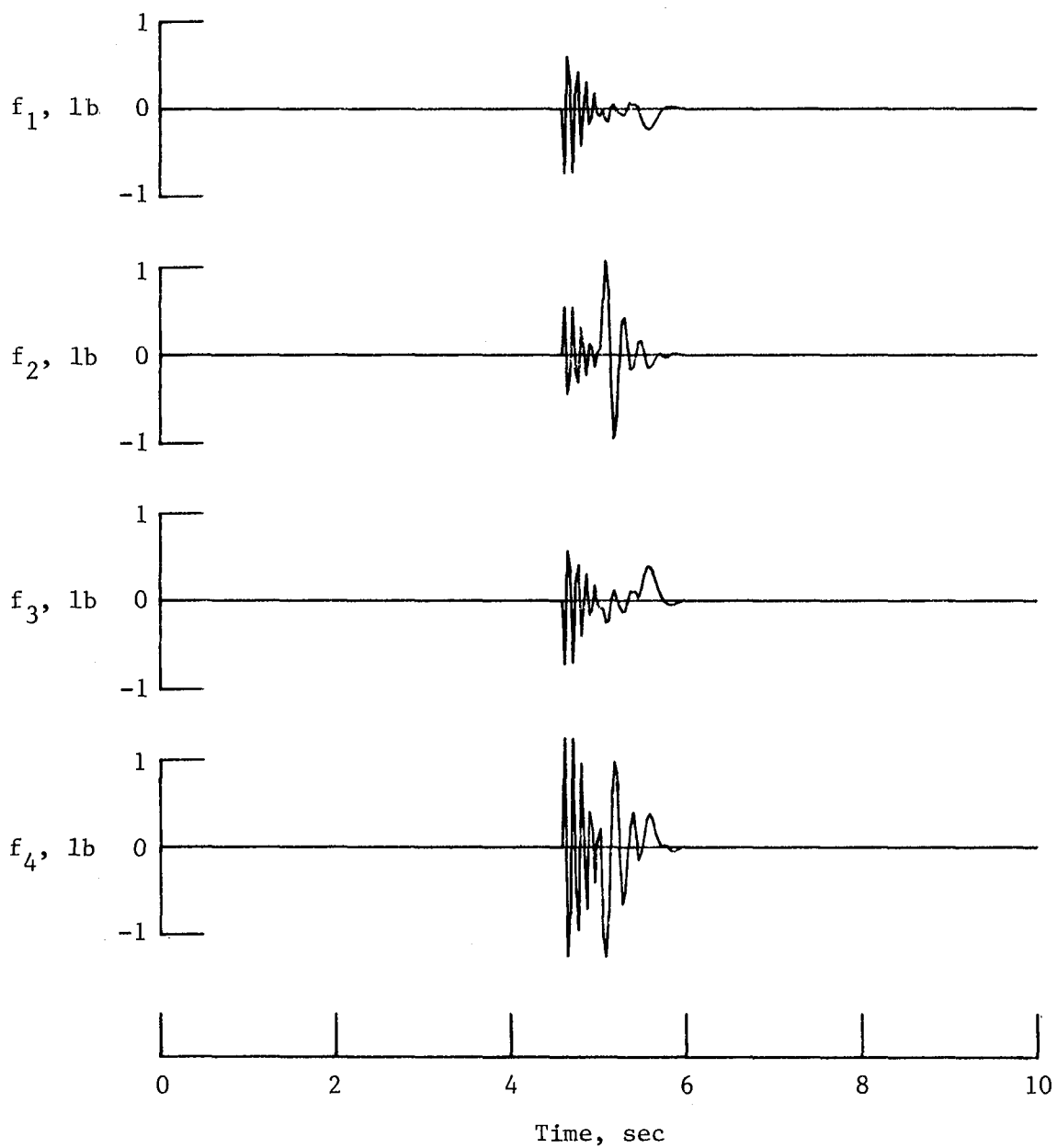
Figure 23. Actuator force commands.
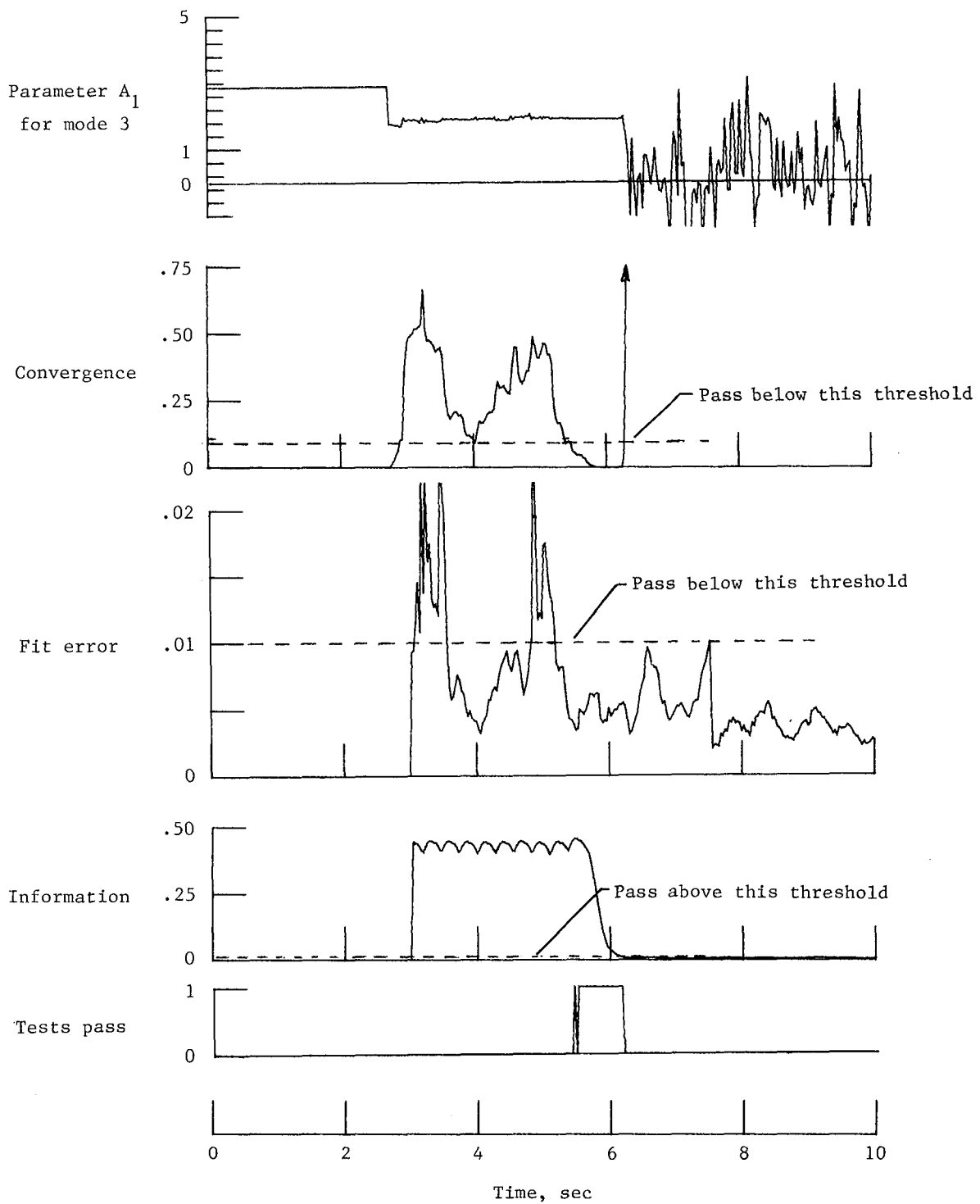
Figure 24. Time histories of test variables for one mode with test thresholds and logic sum of tests indicated.
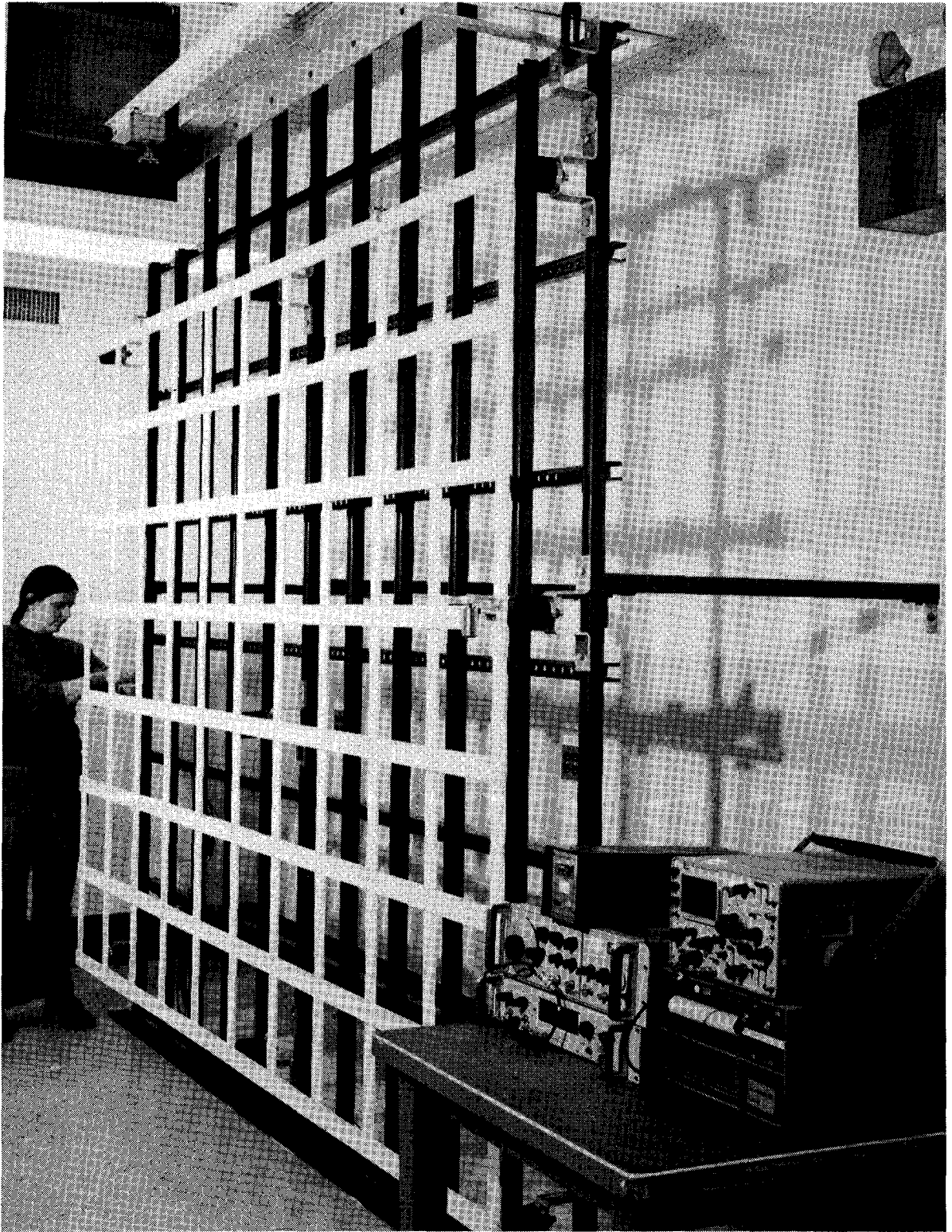
L-82-12,048

Figure 25. Photograph of flexible-grid experimental apparatus.
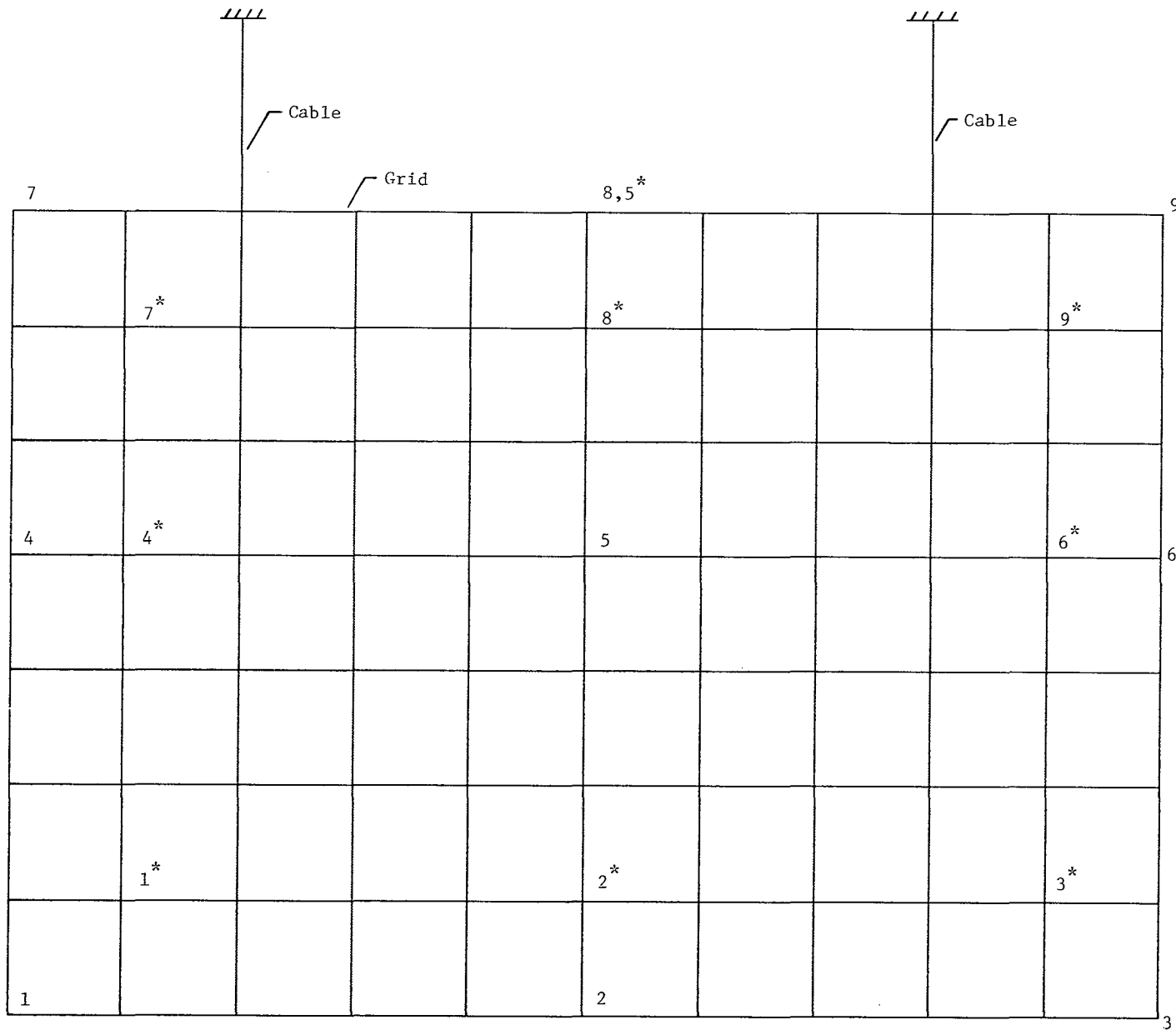
Figure 26. Schematic diagram of grid structure with sensor and actuator locations. Asterisks indicate simulation.
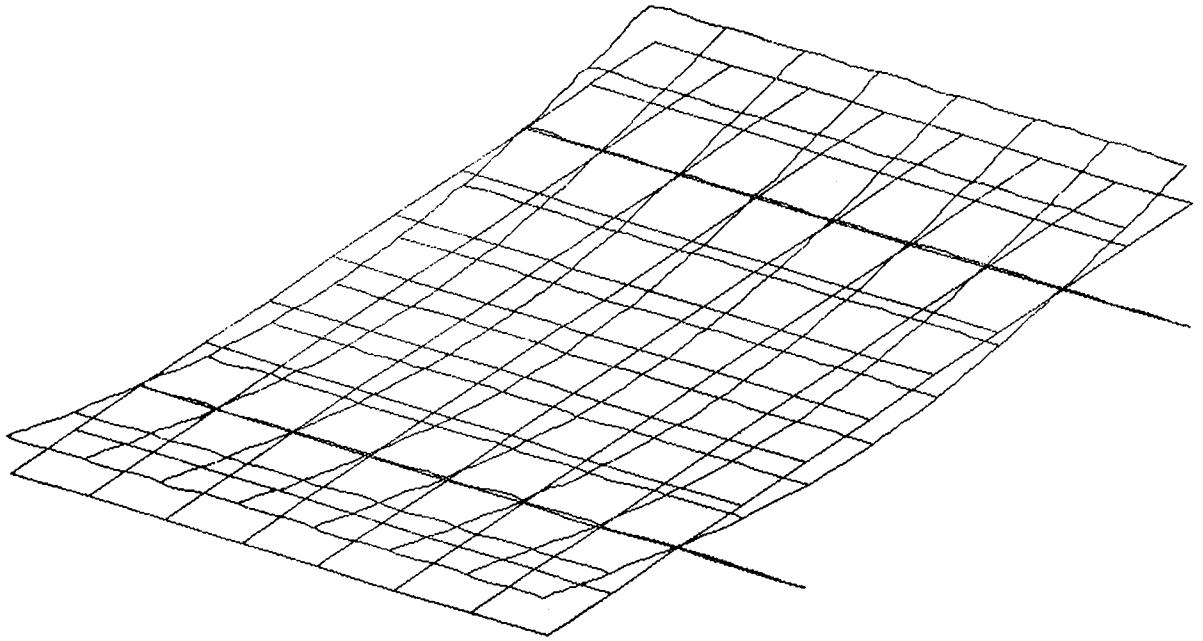
(a) First flexible mode shape. Frequency, 2.299 Hz.
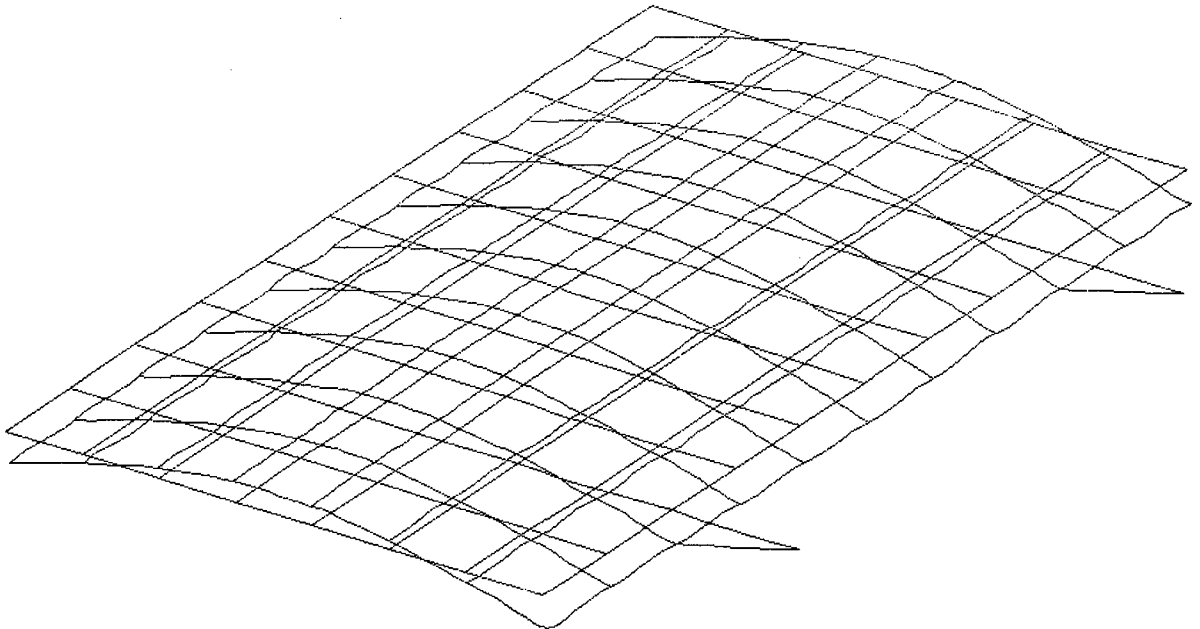
(b) Second flexible mode shape. Frequency, 4.791 Hz.

Figure 27. First four flexible mode shapes for the grid.
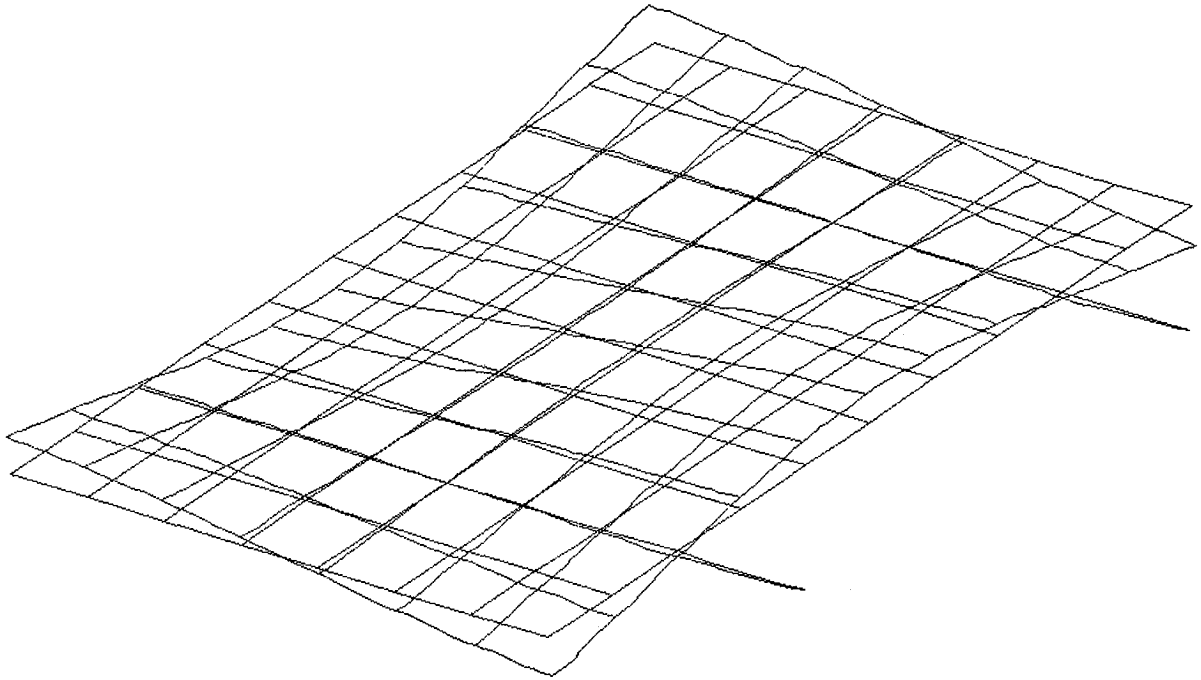
(c) Third flexible mode shape. Frequency, 5.933 Hz.
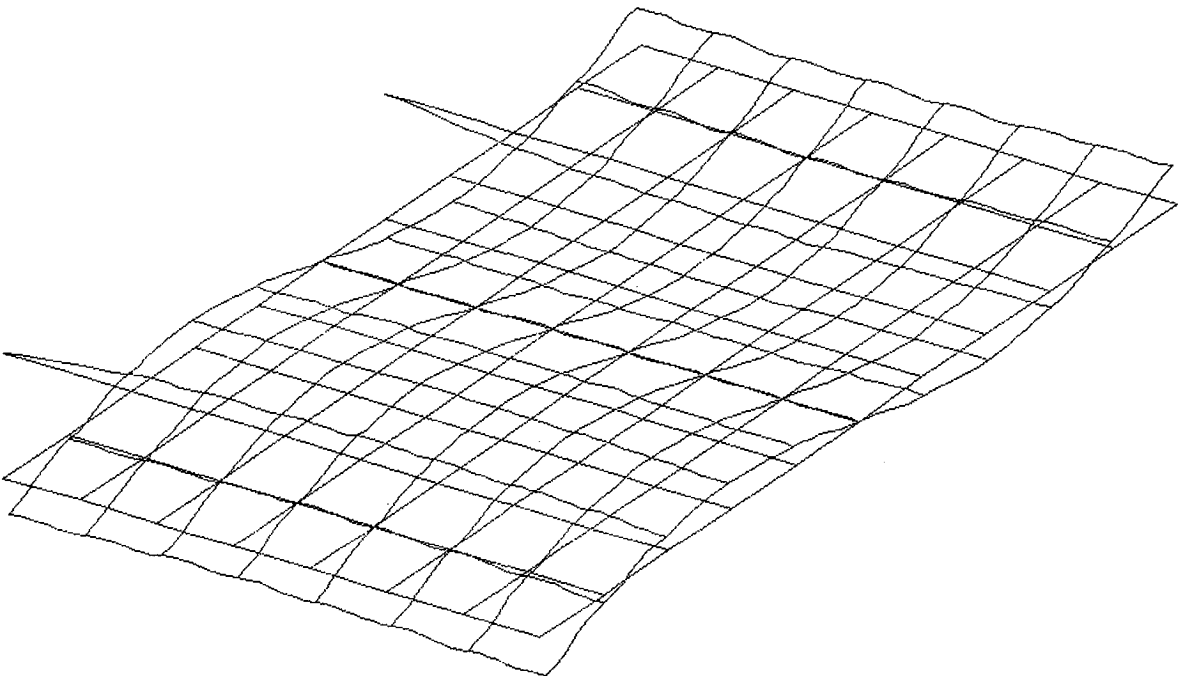
(d) Fourth flexible mode shape. Frequency, 6.297 Hz.

Figure 27. Concluded.
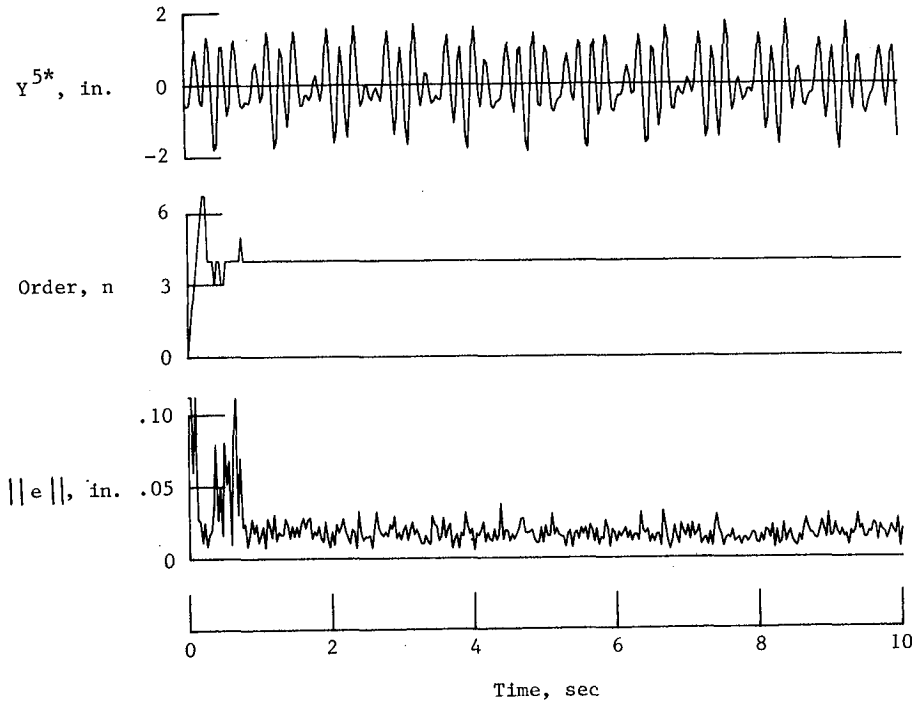
Figure 28. Simulation time histories of sensor 5* as well as lattice-filter order estimate and norm of estimation error for entire measurement vector.
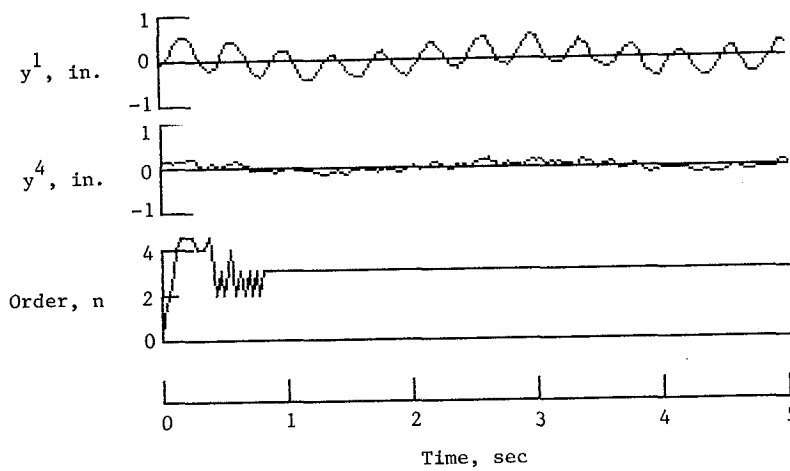

Figure 29. Sensors 1 and 4 from experimental tape 5 and estimate of signal order obtained by lattice filter.
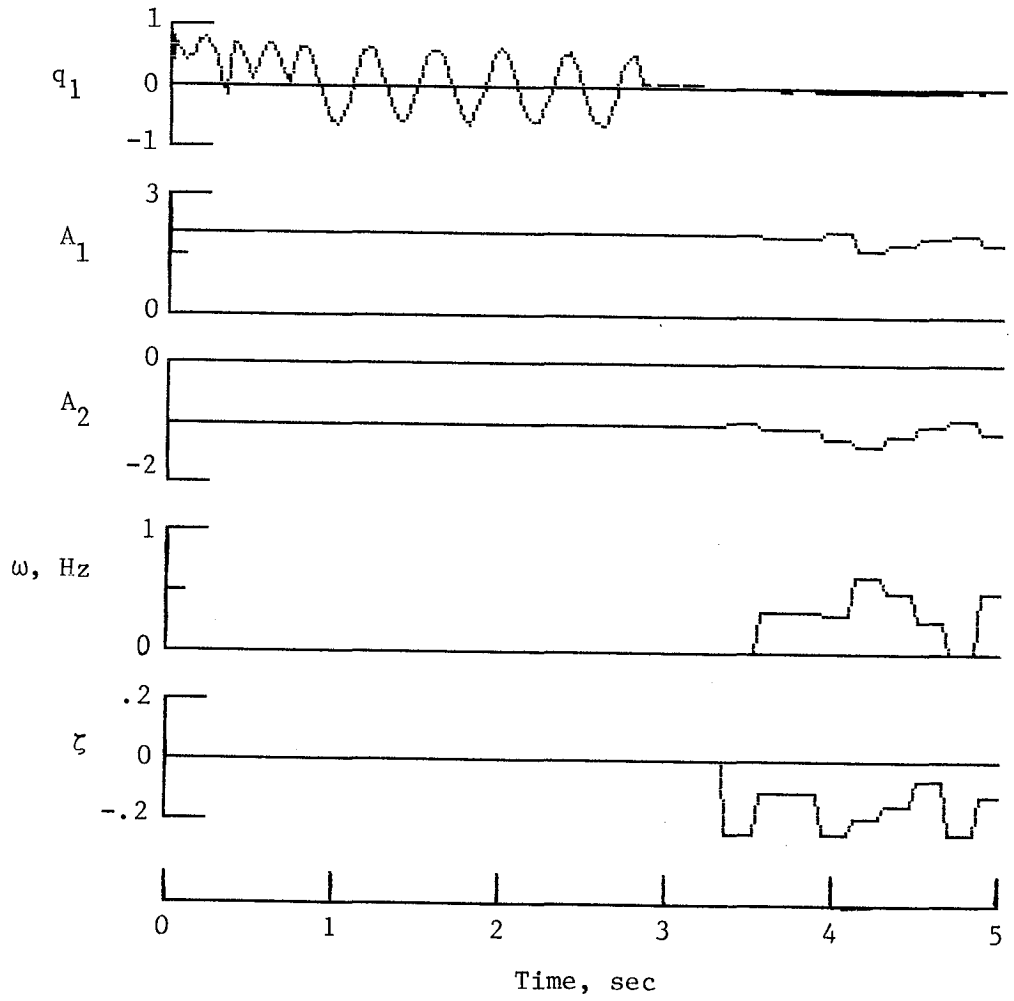
(a) First mode.

Figure 30. Characteristics of modes identified from experimental tape 5.
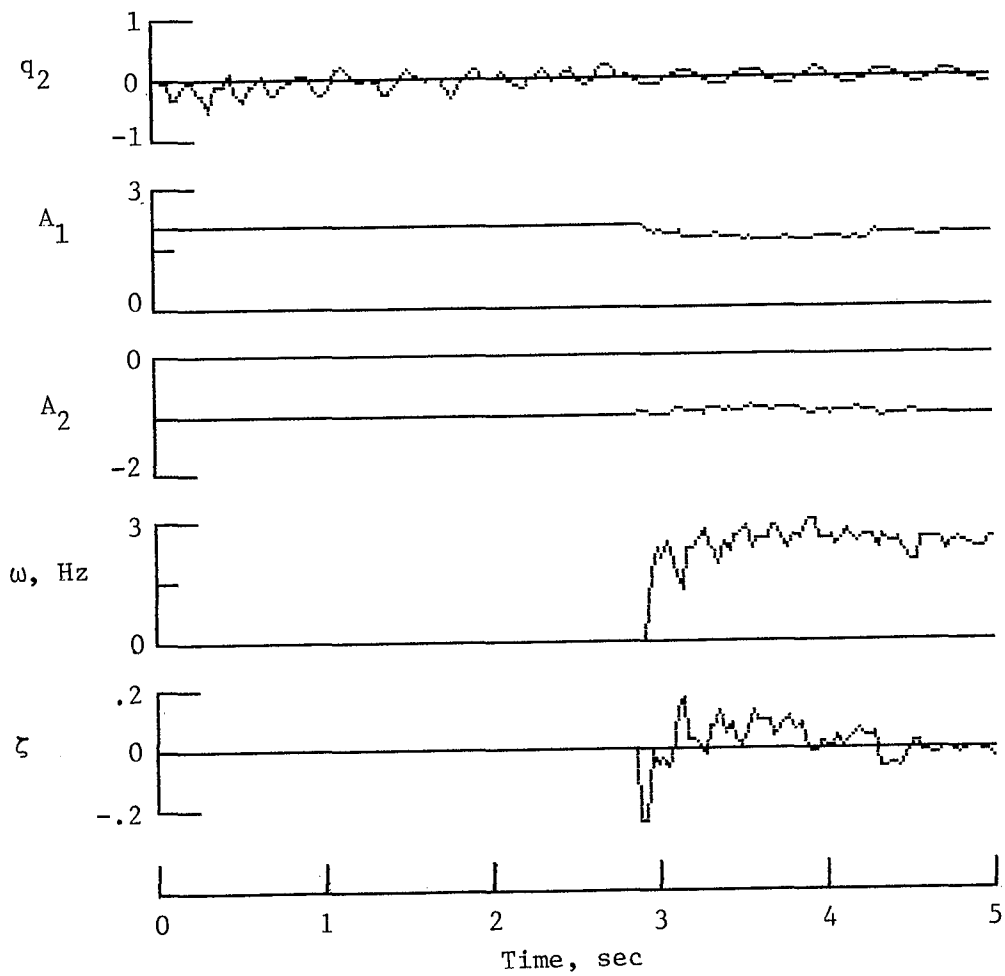
(b) Second mode.

Figure 30. Continued.
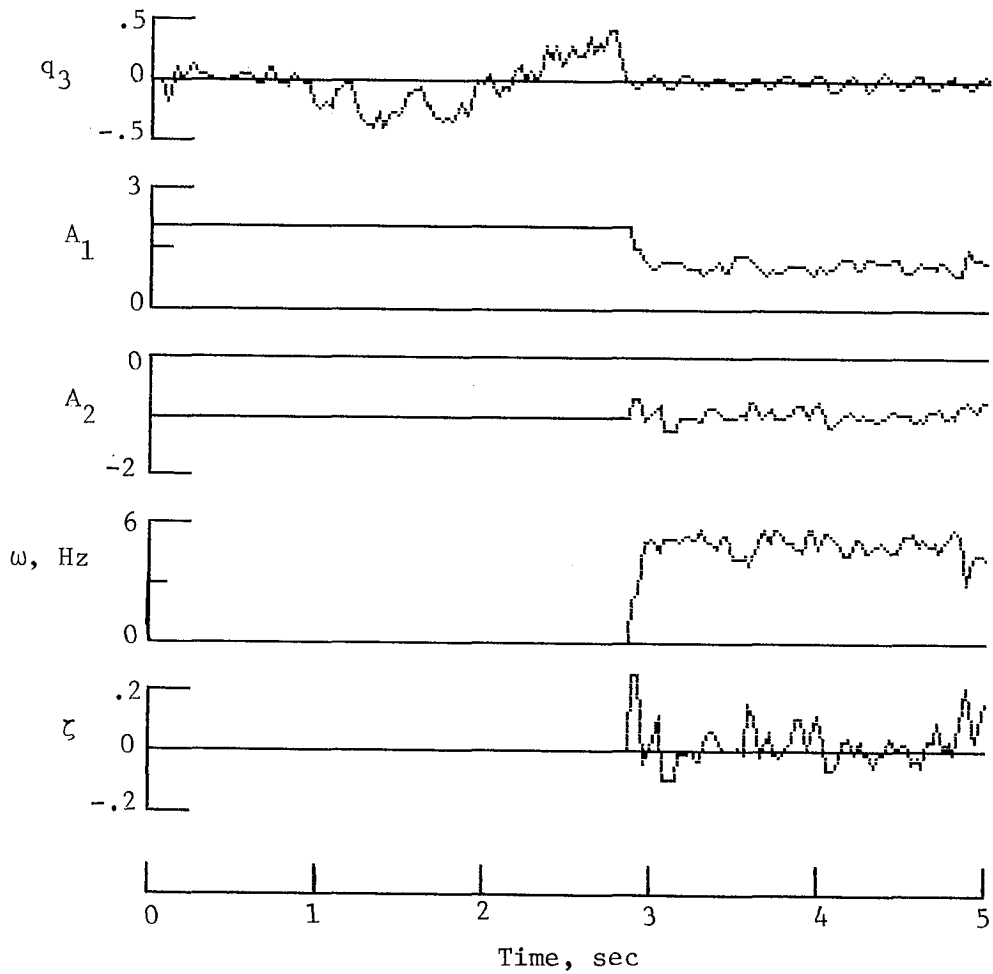
(c) Third mode.

Figure 30. Concluded.

1. Report No. NASA TP-2371	2. Government Accession No.	3. Recipient's Catalog No.
4. Title and Subtitle ADAPTIVE IDENTIFICATION AND CONTROL OF STRUCTURAL DYNAMICS SYSTEMS USING RECURSIVE LATTICE FILTERS		5. Report Date January 1985
		6. Performing Organization Code 506-57-13-03
7. Author(s) N. Sundararajan, Raymond C. Montgomery, and Jeffrey P. Williams		8. Performing Organization Report No. L-15737
9. Performing Organization Name and Address NASA Langley Research Center Hampton, VA 23665		10. Work Unit No.
		11. Contract or Grant No.
12. Sponsoring Agency Name and Address National Aeronautics and Space Administration Washington, DC 20546		13. Type of Report and Period Covered Technical Paper
		14. Sponsoring Agency Code

15. Supplementary Notes

N. Sundararajan: NRC-NASA Resident Research Associate, now on leave from the Indian Space Research Organization.

16. Abstract

This report presents a new approach for adaptive identification and control of structural dynamic systems by using least-squares lattice filters that are widely used in the signal processing area. Testing procedures for interfacing the lattice-filter identification methods and modal control method for stable closed-loop adaptive control have been presented. The methods have been illustrated for a free-free beam and for a complex flexible grid, with the basic control objective being vibration suppression. The approach has been validated by using both simulations and experimental facilities available at the Langley Research Center.

17. Key Words (Suggested by Authors(s)) Adaptive control Lattice filters ARMA identification Free-free beam Flexible grid Experimental results	18. Distribution Statement Unclassified—Unlimited Subject Category 18		
19. Security Classif.(of this report) Unclassified	20. Security Classif.(of this page) Unclassified	21. No. of Pages 50	22. Price A03

National Aeronautics and
Space Administration

Washington, D.C.
20546

Official Business
Penalty for Private Use, $300

THIRD-CLASS BULK RATE

NASA

If Undeliverable (Section 158
Postal Manual) Do Not Return